A *Bartonella* effector acts as signaling hub for intrinsic STAT3 activation to trigger anti-inflammatory responses

Isabel Sorg, [1] Christoph Schmutz, [1,2] Yun-Yueh Lu, [1,3] Katja Fromm, [1] Lena K. Siewert, [1] Alexandra Bögli, [1] Kathrin Strack, [1,4] Alexander Harms, [1] and Christoph Dehio[1,5,*]

Highlights

- *Bartonella* effector BepD impairs TNF-α secretion and stimulates IL-10 secretion
- STAT3 is recruited to tyrosine-phosphorylated EPIYA motifs in BepD
- BepD serves as signaling hub for c-Abl-dependent STAT3 phosphorylation on Y_{705}
- BepD-mediated STAT3 activation pathway is independent from canonical JAK signaling

In brief

In this study Sorg et al. demonstrate that tyrosine phosphorylation of the host-targeted *Bartonella henselae* effector BepD facilitates STAT3 binding and activation via c-Abl-dependent phosphorylation of Y_{705}. This intrinsic pathway for STAT3 activation hampers pro-inflammatory and initiates anti-inflammatory responses, thereby promoting the chronic life style of the pathogen.

Graphical abstract:

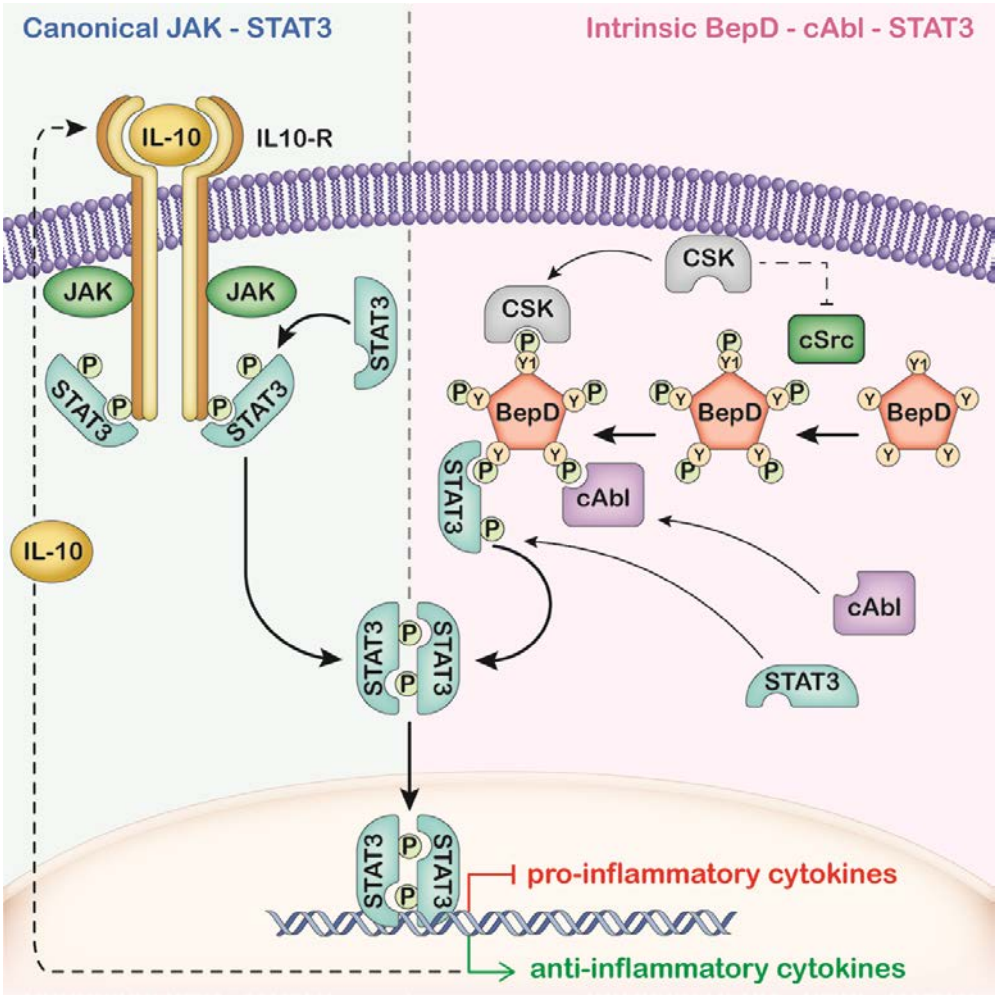

A *Bartonella* effector acts as signaling hub for intrinsic STAT3 activation to trigger anti-inflammatory responses

Isabel Sorg, [1] Christoph Schmutz, [1,2] Yun-Yueh Lu, [1,3] Katja Fromm, [1] Lena K. Siewert, [1] Alexandra Bögli, [1] Kathrin Strack, [1,4] Alexander Harms, [1] and Christoph Dehio[1,5,*]

[1]Biozentrum, University of Basel, 4056 Basel, Switzerland

[2]current address: Bioconcept, 4123 Allschwil, Switzerland

[3]current address: HiFiBiO Therapeutics, 201203 Pudong New Area, China

[4]current address: iOmx Therapeutics AG, 82152 Martinsried, Germany

[5]Lead Contact

*Correspondence: christoph.dehio@unibas.ch

SUMMARY

Chronically infecting pathogens avoid clearance by the innate immune system by promoting premature transition from an initial pro-inflammatory response towards an anti-inflammatory tissue-repair response. STAT3, a central regulator of inflammation, controls this transition and thus is targeted by numerous chronic pathogens, but our understanding of underlying molecular mechanisms is limited. Here we show that the host-targeted effector BepD of the chronic bacterial pathogen *Bartonella henselae* establishes a novel pathway for STAT3 activation, thereby impairing secretion of pro-inflammatory TNF-α and stimulating secretion of anti-inflammatory IL-10. Tyrosine phosphorylation of EPIYA-related motifs in BepD facilitates STAT3 binding and activation via c-Abl-dependent phosphorylation of Y_{705}. The tyrosine-phosphorylated scaffold of BepD thus represents a signaling hub for intrinsic STAT3 activation that is independent from canonical STAT3 activation via transmembrane receptor-associated Janus kinases. We anticipate that our findings on a molecular shortcut to STAT3 activation will inspire new treatment options for chronic infections and inflammatory diseases.

INTRODUCTION

Innate immune detection of pathogens by mammalian cells depends on 'pattern recognition receptors' (PRRs) which recognize conserved molecular structures called 'pathogen-associated molecular patterns' (PAMPs) (Mogensen, 2009). Gram-negative bacteria are sensed primarily via binding of lipopolysaccharide (LPS) or lipoproteins to their cognate receptors Toll-like-receptor 4 (TLR4) and 2 (TLR2), respectively (Aderem and Ulevitch, 2000). TLR4 and TLR2 signaling pathways converge on the expression and secretion of pro-inflammatory cytokines like TNF-α and IL-6. The resulting inflammatory response involves bactericidal M1 macrophages that promote pathogen restriction and clearance, but also provokes significant tissue damage (Murray et al., 2014). Down-regulation of this pro-inflammatory response and concomitant up-regulation of an anti-inflammatory response involving IL-10 secretion and alternatively activated M2 macrophages then promotes tissue repair and resolution of inflammation (Murray et al., 2014).

The switch from pro-inflammatory to anti-inflammatory signaling is controlled by the transcription factor STAT3 which plays also key roles in regulating cell growth and survival (Hillmer et al., 2016; Yu et al., 2009). In response to IL-6 and IL-10, receptor-associated Janus kinases (JAK) phosphorylate STAT3 on Y_{705}. Alternatively, Y_{705} is phosphorylated by c-Abl or Src-family non-receptor tyrosine kinases (Allen et al., 2011; Garcia et al., 2001). STAT3 phosphorylated on Y_{705} homo-dimerizes and translocates to the nucleus where it activates a complex transcriptional program.

Canonical JAK-STAT3 signaling modulates expression of both pro-inflammatory (e.g., IL-6) and anti-inflammatory cytokines (e.g., IL-10). The temporal switch from pro-inflammatory to anti-inflammatory signaling critically depends on differential STAT3 activation (Murray, 2007). Due to its central role in inflammation control, STAT3 activity is manipulated by numerous infectious agents including viruses (Suarez et al., 2018) as well as the bacterial pathogens *Helicobacter pylori* (Menheniott et al., 2015) and *Salmonella* Typhimurium (Hannemann et al., 2013; Jaslow et al., 2018). However, our understanding of the molecular mechanisms underlying STAT3 activation by these infectious agents is limited.

Bartonella spp. are stealth bacterial pathogens that cause chronic infections in mammals (Harms and Dehio, 2012). To modify the immune response in favor of establishing chronic infection, these pathogens translocate multiple *Bartonella* effector proteins (Beps) into host cells via the VirB/VirD4 type-IV-secretion system (T4SS; Schulein et al., 2005; Wagner and Dehio, 2019). The major zoonotic pathogen *Bartonella henselae*, which causes cat-scratch-disease and other clinical manifestations in humans, translocates a cocktail of seven Beps (i.e., BepA-BepG; Schulein et al., 2005). BepD-BepF belong to an effector class characterized by tandem-repeated sequence variants of the EPIYA motif originally defined in CagA of *H. pylori* (Backert and Selbach, 2005; Hayashi et al., 2013; Schulein et al., 2005; Selbach et al., 2009; Xu et al., 2010). Within host cells, these EPIYA-related motifs become tyrosine-phosphorylated by Src-family kinases, which facilitates specific interactions with SH2 domain-containing proteins, thereby manipulating host cell signaling.

In this study, we reveal that BepD uses an array of phosphorylated EPIYA-related motifs as signaling hub to induce STAT3 activation in immune cells through a novel c-Abl-dependent intrinsic pathway which impairs the pro-inflammatory response and provokes a potent anti-inflammatory response. Our findings do not only highlight the importance of STAT3 regulation in chronic infections but might also inspire new approaches to control inflammatory diseases.

RESULTS

BepD impairs *Bartonella*-induced TNF-α secretion

Superficial skin inoculation typically represents the initial step of human infection by *B. henselae* (Harms and Dehio, 2012). At this dermal site of infection, dendritic cells (DCs) are likely the first host cell type to interact with this stealth pathogen (Harms and Dehio, 2012). The pro-inflammatory response of DCs to *B. henselae* is limited by the low potency of its PAMPs, and might be further impaired by the activities of Beps. *B. henselae* triggers TNF-α secretion mainly via lipoprotein-mediated activation of TLR2 (Vermi et al., 2006), while the converging TLR4 signaling pathway is barely activated due to the unusual chemical structure of *B. henselae* LPS (Vermi et al., 2006; Zahringer et al., 2004; Figure 1A). To test whether the modest pro-inflammatory response to *B. henselae* PAMPs is impaired in dependence of the VirB/VirD4 T4SS and translocated Beps, we infected the mouse DC line JAWS II with *B. henselae* Houston-1 Sm^R (Schmid et al., 2004) used as wild-type strain throughout this study or with isogenic mutant derivatives for 6 h at a multiplicity of infection (MOI) of 50. Compared to the low level of TNF-α secretion resulting from infection by wild-type bacteria (<60 pg ml^{-1}), TNF-α secretion was significantly increased by infection with the type-IV-secretion-deficient *ΔvirD4* mutant or the Bep-deficient *ΔbepA-G* mutant (>110 pg ml^{-1}; Figure 1B). A similar differential response was observed for primary mouse splenic DCs, albeit at lower TNF-α levels (Figure S1A, B). The observed VirD4- and Bep-dependent impairment of TNF-α secretion was likewise observed when JAWS II cells (Figure 1C) or mouse splenic DCs (Figure S1C) were co-stimulated at 4 h post infection (hpi) with exogenous *E. coli* LPS as potent TLR4 ligand, which robustly increased TNF-α levels for all infection conditions.

JAWS II cell infection with co-stimulation by *E. coli* LPS was chosen as experimental model to further characterize Bep-dependent impairment of TNF-α secretion. To test if a single Bep mediates this effect we separately expressed each of the seven Beps from a plasmid in the Bep-deficient *ΔbepA-G* background (Figure 1D). BepD impaired TNF-α secretion to a similar extend as wild-type bacteria, while no other Bep displayed a

discernable inhibitory effect on TNF-α secretion. We thus concluded that BepD mediates the impairment of TNF-α secretion observed for infection with wild-type *B. henselae*.

Five conserved EPIYA-related phosphorylation motifs in BepD are required to impair TNF-α secretion

To develop a rational for functional analysis of BepD by mutagenesis we performed a detailed bioinformatic analysis (Figures 1E, F, G and S2A). BepD of *B. henselae* Houston-1 contains a C-terminal 'Bep intracellular delivery' (BID) domain that serves as signal for VirB/VirD4-dependent translocation (Schulein et al., 2005) and at its N-terminus two nearly identical tyrosine phosphorylation domains of 179 aa (Harms et al., 2017; Schulein et al., 2005; Selbach et al., 2009). Each of these pY and pY' domains contain an array of nine EPIYA-related phosphorylation motifs for which the tyrosine residues were sequentially numbered Y1-Y9 or Y1'-Y9', respectively (Figure 1E). The pY domain is highly conserved among BepD homologues within and beyond *Bartonella* species, while only a subset of them contains also a pY' domain or at least parts of it (Figure 1F). BepD was found in two major variants regarding the arrangement of pY'/pY domains, once with a tandem of both domains (represented by strains Houston-1 and U4) and once with pY only (represented by A242 and Zeus; Figure 1F). Alignment of the pY and pY' domains of strain Houston-1 with the pY domain of strain A242 demonstrated full conservation of all nine EPIYA-related motifs (Figure 1G, see Figure S2A for alignment of all 11 BepD homologs presented in Figure 1F). This bioinformatic analysis suggests that the pY' domain of *B. henselae* Houston-1 BepD may be structurally and functionally redundant with the evolutionarily more conserved pY domain and thus may not be required for BepD function. Indeed, JAWS II cells infected with *B. henselae* *ΔbepA-G* derivatives expressing either full-length BepD or $BepD_t$ truncated for the N-terminal pY' domain displayed similar decreases of *E. coli* LPS-triggered TNF-α secretion (Figure 1H). In contrast, expression of the BepD BID domain alone that still is translocated by VirB/VirD4 (Schulein et al., 2005) did not impair TNF-α secretion, indicating a critical role of the pY domain in mediating the BepD anti-inflammatory activity.

Due to its lack of domain redundancy $BepD_t$ was chosen for further functional analysis. Ectopic expression in host cells was used to test if $BepD_t$ impairs TNF-α secretion in absence of any other bacterial factor. To this end we generated stable transgenic JAWS II cell lines by lentiviral transduction that under control of the doxycycline-inducible promoter pTF express either GFP-tagged $BepD_t$ (GFP-$BepD_t$ wt) or GFP alone (GFP) (Figure 1I, left panel). Compared to GFP, GFP-$BepD_t$ wt significantly reduced secretion of TNF-α triggered by *E. coli* LPS, indicating that $BepD_t$ alone is indeed sufficient to impair pro-inflammatory signaling.

Next, we used the JAWS II ectopic expression model to assess which tyrosines of the nine conserved EPIYA-related motifs of $BepD_t$ are critical for the observed inflammation-modulatory activity. We introduced single Y-to-F exchange mutants for each of Y1 to Y9 of GFP-$BepD_t$ wt and generated stably transduced expression cell lines. Upon doxycycline induction and stimulation with *E. coli* LPS, Y1F and Y4F were found to have lost most and Y5F, Y6F and Y7F to have lost essentially all of the inhibitory activity on TNF-α secretion in comparison to GFP-$BepD_t$ wt (Figure 1I, right panel). These five Y-to-F loss-of-function mutations were combined in the quintuple mutant GFP-$BepD_t$ 5Ymut that was devoid of any detectable activity to inhibit TNF-α secretion. Expression of all GFP-fusion proteins was detected by immunoblot (Figure 2E; antibody GFP).

Tyrosine-phosphorylated EPIYA-related motifs in BepD are required for recruitment and phosphorylation of STAT3 on Y_{705}

A previous study on the interactome of phosphorylated EPIYA-related motifs in bacterial effectors revealed that several SH2 domain-containing signaling proteins interacted with *B. henselae* BepD Y1 and Y1' in a tyrosine phosphorylation-dependent manner (Selbach et al., 2009). Interestingly, Y1 is one of five tyrosines involved in the inhibition of pro-inflammatory responses by BepD (Figure 1I). To extend the identification of cellular interactors to all five functionally relevant tyrosines of $BepD_t$ we performed two orthogonal proteomics approaches, i.e., interactomics and phosphoproteomics. In both approaches we compared

157 the functional GFP-BepD$_t$ wt protein with the inactive quintuple Y-to-F mutant protein
158 GFP-BepD$_t$ 5Ymut. In the interactomics approach, interactors of phosphorylated Y1, Y4, Y5,
159 Y6 and Y7 motifs were identified by pull-down of GFP-BepD$_t$ wt or GFP-Bep$_t$ 5Ymut from
160 JAWS II cell lysates with GFP-nanobodies, followed by proteolytic digestion and mass-
161 spectrometric analysis. Volcano plot analysis revealed 12 specific interactors that were
162 significantly enriched in the GFP-BepD$_t$ pull-down fraction (Figure 2A). Eight of those contain
163 SH2 domains, suggesting that their binding is dependent on tyrosine phosphorylation of the
164 respective EPIYA-related motifs. Among those were CSK and SHP2 previously reported to
165 interact with Y1 of BepD (Selbach et al., 2009), thus validating our experimental approach.
166 STAT3 and c-Abl represent other interesting SH2 domain-containing proteins that specifically
167 interacted with GFP-BepD$_t$ wt and thus represent compelling candidates for the BepD-
168 dependent inflammation control pathway.
169 Quantitative phosphoproteomics of JAWS II cells expressing GFP-BepD$_t$ wt or GFP-
170 BepD$_t$ 5Ymut was performed by tryptic digest of cell lysates, followed by phosphopeptide
171 enrichment by TiO_2 coupled with mass spectrometry as described previously (Schmutz et al.,
172 2013). Volcano plot analysis identified 27 phosphopeptides with significant changes in
173 phosphorylation levels in dependence of GFP-BepD$_t$ wt. Among those, 19 phosphopeptides
174 from 12 proteins displayed increased and eight phosphopeptides from eight proteins
175 decreased levels of phosphorylation (Figure 2B). Presentation of the hits from both
176 approaches as STRING protein interaction network (Szklarczyk et al., 2019) displayed
177 several interconnected functional modules (Figure 2C). STAT3 was the only protein identified
178 by both proteomic approaches. Notably, phosphoproteomics identified phosphorylation of
179 STAT3 on Y_{705} which is known to provoke STAT3 dimerization, nuclear translocation and
180 transcriptional activity (Wen et al., 1995). STAT3 was also found to be phosphorylated on
181 serine S_{727}, a modification known to enhance its transcriptional activity (Wen et al., 1995). A
182 pull-down experiment demonstrated that STAT3 and its Y_{705}-phosphorylated form associated
183 specifically with GFP-BepD$_t$ wt, while no interaction was detectable for GFP-BepD$_t$ 5Ymut
184 (Figure 2D, lanes 5 and 6). Consistent with the hypothesis that STAT3 is recruited to BepD

via specific SH2 domain – phosphotyrosine interaction, only GFP-BepD$_t$ wt was found to be tyrosine-phosphorylated, while no tyrosine phosphorylation was detectable for the quintuple Y-to-F mutant GFP-BepD$_t$ 5Ymut (Figure 2D, lanes 1 and 2 or 5 and 6; antibody p-Tyr). Moreover, for the set of JAWS II cell lines ectopically expressing individual Y-to-F mutants of the nine EPIYA-related motifs in GFP-BepD$_t$ we observed that loss of inhibition of TNF-α secretion (Figure 1I) correlated with loss of STAT3 phosphorylation (Figure 2E), i.e., intermediate losses for Y1 and Y4 and almost complete losses for Y5, Y6 and Y7.

In summary, an array of five distinct EPIYA-related phosphorylation motifs in BepD constitutes a signaling platform for STAT3 activation that recruits SH2 domain-containing signaling proteins, including STAT3 and upstream tyrosine kinases such as c-Abl.

BepD mediates STAT3 phosphorylation independent of auto- or paracrine cytokine signaling or transmembrane signaling by JAK

Since *H. pylori* was shown to activate STAT3 signaling via an IL-10-dependent auto- and paracrine feedforward loop (Rizzuti et al., 2015), we tested whether inhibition of cytokine secretion via treatment with brefeldin A had a negative impact on BepD-dependent STAT3 phosphorylation on Y_{705}. JAWS II cells expressing GFP-BepD$_t$ wt were either left untreated or treated with *E. coli* LPS to induce the expression of pro-inflammatory cytokines such as IL-6 (Figure S3). Treatment with brefeldin A led to an accumulation of intracellular IL-6 demonstrating the efficacy of secretion inhibition in this experimental setting. However, brefeldin A did not inhibit GFP-BepD$_t$ wt-dependent STAT3 Y_{705} phosphorylation (Figure S3), indicating that BepD-dependent STAT3 activation in JAWS II cells occurs independently of an auto- or paracrine loop of cytokine secretion and thus has to occur intrinsically.

Next, we used the JAK inhibitor ruxolitinib (Harrison and Vannucchi, 2012) to test if STAT3 phosphorylation on Y_{705} via the canonical JAK-STAT3 pathway is involved in BepD-dependent STAT3 activation (Figure 3A). Although ruxolitinib efficiently blocked IL6-induced phosphorylation of STAT3 on Y_{705} (Figure 3B), it had no detectable effect on the robust Y_{705} phosphorylation induced by ectopic expression of GFP-BepD$_t$ wt in JAWS II cells (Figure 3B)

nor did this inhibitor treatment block GFP-BepD$_t$ wt-induced reduction of TNF-α secretion (Figure 3C). Taken together, we conclude that BepD-dependent STAT3 phosphorylation on Y_{705} occurs by a JAK-independent pathway.

The tyrosine kinase c-Abl phosphorylates STAT3

Identification of c-Abl as BepD interactor (see Figure 2) and previous reports indicating that c-Abl can activate STAT3 by Y_{705} phosphorylation (Allen et al., 2011) prompted us to test if c-Abl is the upstream kinase responsible for BepD-dependent STAT3 phosphorylation. For this purpose, JAWS II cells expressing either functional GFP-BepD$_t$ wt or the inactive GFP-BepD$_t$ 5Ymut were treated with the Abl-specific inhibitor imatinib (Druker et al., 2001), followed by cell lysis, pull-down with GFP-specific nanobodies and immune blot analysis. Strikingly, imatinib treatment strongly (by 70%) reduced GFP-BepD$_t$ wt-induced STAT3 phosphorylation on Y_{705} [Figure 3D, lanes 1 and 2; antibody p-STAT (Y_{705})], while phosphorylation levels of immunoprecipitated GFP-BepD$_t$ wt were only moderately reduced (by 33%)(Figure 3D; lanes 9 and 10, antibody p-Tyr; Figure S3B). Importantly, corresponding amounts of STAT3 were co-immunoprecipitated with GFP-BepD$_t$ wt in imatinib- or mock-treated conditions (45% reduction with imatinib), indicating that recruitment of STAT3 to tyrosine-phosphorylated BepD was only moderately affected by imatinib treatment (Figure 3D; lanes 9 and 10, antibody STAT3; Figure S3B), while the level of Y_{705} phosphorylation was greatly reduced by 80% [Figure 3D; lanes 9 and 10, antibody p-STAT3 (Y_{705}); Figure S3B]. These data indicate that c-Abl recruited to tyrosine-phosphorylated BepD is largely responsible for STAT3 phosphorylation on Y_{705}. In contrast, c-Abl contributes only moderately to tyrosine-phosphorylation of BepD. Rather, BepD phosphorylation may result primarily from c-Src (Guye, 2005).

Next, we tested whether the reduction of GFP-BepD$_t$ wt-dependent STAT3 phosphorylation by imatinib (Figure 3D and E) translates into an alleviation of GFP-BepD$_t$ wt-dependent impairment of TNF-α secretion (Figure 3F). Imatinib treatment of GFP-BepD$_t$ wt-expressing JAWS II cells indeed increased TNF-α secretion significantly to a level

comparable to the elevated level observed in the GFP-$BepD_t$ 5Ymut-expressing JAWS II control cell line. Importantly, imatinib treatment did not appear to alter TNF-α secretion in this control cell line expressing an inactive BepD variant, indicating that the observed imatinib inhibition of c-Abl is specific for the BepD-dependent STAT3 phosphorylation pathway.

BepD induces early IL-10 secretion in macrophages

Until discovery of the novel BepD/c-Abl-dependent pathway of STAT3 activation we had focused our characterization of innate inflammation control by BepD on the impairment of pro-inflammatory responses; i.e., the inhibition of TNF-α secretion. However, sustained activation of STAT3 not only impairs pro-inflammatory responses, but also specifically triggers secretion of the potent anti-inflammatory cytokine IL-10. A time-course of BepD-dependent STAT3 phosphorylation upon infection of JAWS II cells with *B. henselae ΔbepA-G* expressing BepD revealed detectable Y_{705}-phosphorylation already 1 hpi followed by a sustained increase of phosphorylation levels (Figure S4A). This kinetics should trigger a sustained IL-10 anti-inflammatory response prone to the establishment of chronic bacterial infection. However, as JAWS II cells are incapable of expressing IL-10 (Jiang et al., 2008a) we tested this hypothesis with macrophages that represent a target cell type for *Bartonella* at later stages of infection (Hong et al., 2017). First, we tested the mouse RAW 264.7 macrophage cell line that is known to be able of mounting a robust IL-10 response (Hobbs et al., 2018). Consistent with JAWS II cells, RAW 264.7 cells displayed phosphorylation of STAT3 on Y_{705} in response to infection with *B. henselae ΔbepA-G* expressing BepD (*ΔbepA-G* + p*bepD*) but not the *ΔbepA-G* mutant (Figure 4A) which was also independent of auto- and paracrine signaling (Figure S4B, C, D). This strong STAT3 activation translated to an even stronger impairment of TNF-α secretion (Figure 4B) than observed in DCs (Figures 1B and S1A). Of note, *B. henselae* PAMPs trigger a robust TNF-α secretion in RAW 264.7 cells (about 1500 pg ml^{-1} for strain *ΔbepA-G*), thus co-stimulation with *E. coli* LPS as used in most experiments with DCs was unnecessary in this macrophage model. Importantly, IL-10 secretion levels displayed an inverse correlation with TNF-α secretion in response to

infection with various *B. henselae* strains (Figure 4B and C), demonstrating a marked increase of IL-10 secretion in dependence of BepD (Figure 4C; ~ 1100 pg ml^{-1} for *ΔbepA-G* + p*bepD* vs. ~ 500 pg ml^{-1} for *ΔbepA-G*). A time-course experiment furthermore showed a significant BepD-dependent increase in IL-10 secretion already at the earliest time-point (4 hpi), that over time was followed by substantial accumulation of IL-10 in the cell culture medium (Figure 4D; > 2000 pg ml^{-1} for *ΔbepA-G* + p*bepD* vs. < 300 pg ml^{-1} for *ΔbepA-G*). Primary mouse bone marrow-derived macrophages (BMM) confirmed the data obtained with RAW 264.7 cells by showing similar BepD-mediated impairment of TNF-α secretion (Figure 4E) and stimulation of IL-10 secretion (Figure 4F). Taken together, these data demonstrate that the BepD/STAT3-dependent inflammation control pathway involves a strong anti-inflammatory IL-10 response in macrophages.

DISCUSSION

Following innate immune sensing of bacterial PAMPs by PRRs, the typical succession of innate pro- and anti-inflammatory responses critically depends on differential STAT3 activation, which is considered to be integrated via JAK-dependent transmembrane cytokine signaling loops. A feedback loop of IL-6 signaling via inactivation of its receptor IL-6R by the STAT3 transcriptional target SOCS3 is considered to shape the transient course of the initial pro-inflammatory response (Murray, 2007). Being a STAT3 transcriptional target itself, IL-10 then mounts a feedforward signaling loop via its SOCS3-insensitive receptor IL-10R, which leads to a sustained anti-inflammatory response (Murray, 2007; see graphical abstract). In contrast to these auto- and paracrine cytokine loops of JAK/STAT3 signaling, BepD takes a shortcut to STAT3 activation via an intrinsic mechanism that potently impairs pro-inflammatory responses (i.e., diminishing of TNF-α secretion) and simultaneously activates a sustained anti-inflammatory response (i.e., stimulation of IL-10 secretion). A molecular model of BepD-mediated STAT3 activation is illustrated by the graphical abstract. The BepD pY domain constitutes a signaling platform formed by a scaffold of five interspersed EPIYA-related motifs (i.e., Y1, Y4, Y5, Y6 and Y7). Upon tyrosine-phosphorylation by Src-family

kinases these EPIYA-related motifs will recruit distinct SH2 domain-containing proteins that facilitate STAT3 activation. The EPLYA motif of Y1 recruits CSK as previously reported for the identical motif in BepE (Selbach et al., 2009). Similar as shown for the mammalian cytoplasmic protein pragmin that binds CSK via an EPIYA-motif, this sequestration of CSK away from its site of activity at the plasma membrane may result in globally enhanced Src-family kinase activity (Safari et al., 2011), thus mediating high steady-state levels of BepD phosphorylation. Recruitment of STAT3 and its kinase c-Abl by at least two of the other phosphorylated EPIYA-related motifs of BepD then triggers STAT3 phosphorylation on Y_{705}, which should upon release from BepD result in homo-dimerization and translocation to the nucleus where STAT3 dimers will mount an anti-inflammatory transcriptional response. Our study thus established a molecular paradigm for STAT3 activation by a bacterial effector protein and implied for the first time, c-Abl as upstream kinase of STAT3 in inflammatory signaling.

The pY domain of *B. henselae* BepD - including the five EPIYA-related motifs that are essential for STAT3 activation - is highly conserved among BepD homologues of other *Bartonella* species (Figures 2F and S2A). Moreover, we observed that BepD homologues of other *Bartonella* species have maintained the capacity to activate STAT3 phosphorylation (Figure S2B). These findings indicate evolutionary conservation of the structure and function of BepD as signaling hub for STAT3 activation, which represents an important anti-inflammatory mechanism for the shared chronic life-style in mammalian hosts. It will be interesting to investigate whether other known bacterial effectors harboring EPIYA-related motifs, which are translocated by diverse pathogenic bacteria to evade pro-inflammatory signaling (Hayashi et al., 2013; Xu et al., 2010), may trigger STAT3 signaling by a similar molecular mechanism as BepD.

A more detailed understanding of the underlying molecular mechanism of STAT3 activation by bacterial EPIYA-related motifs may also pave the way for medical application in the context of inflammation control.

ACKNOWLEDGMENTS

We thank the Proteomics Core Facility of the Biozentrum for performing mass spectrometry analyses and Maxime Quebatte for critical reading of the manuscript. This work was supported by grant 310030A_173119 from the Swiss National Science Foundation (SNSF, www.snf.ch) to C.D.

AUTHOR CONTRIBUTIONS

I.S., C.S., and C.D. designed the conceptual framework of the study and experiments. Y-Y.L. initiated the project and cloned expression constructs. C.S. designed and analyzed mass spectrometry experiments. I.S., Y-Y.L., K.F., L.S., A.B. and K.S. performed and analyzed *in vitro Bartonella* infection experiments, cell biological assays and biochemical assays. A.H. performed bioinformatic analyses of *bepD* gene sequences. I.S. and C.D. wrote the manuscript.

DECLARATION OF INTERESTS

The authors have no competing financial interest to declare.

FIGURE TITLES AND LEGENDS

Figure 1. BepD abrogates *B. henselae*-induced TNF-α secretion

(A) The pro-inflammatory response of dendritic cells (DCs) to the stealthy pathogen *B. henselae* is limited by the low potency of its PAMPs, and may be further abrogated by *Bartonella* effector proteins (Beps) translocated by the VirB/VirD4 T4SS. *B. henselae* triggers TNF-α secretion mainly via activation of TLR2 by lipoproteins, while the converging TLR4 signaling pathway is barely activated by *B. henselae* LPS. To robustly assay for interference with pro-inflammatory signaling, TNF-α secretion was co-stimulated by *E. coli* LPS as potent TLR4 ligand. **(B-D)** Mouse dendritic JAWS II cells were infected at MOI=50 with *B. henselae* wild-type, the Type-IV-secretion-deficient mutant *ΔvirD4*, the Bep-deficient mutant *ΔbepA-G* or *ΔbepA-G* derivatives expressing individual Beps from a plasmid (p*bepA*-p*bepG*). At 6 hours post infection (hpi), secreted TNF-α was quantified by ELISA. **(C, D)** Cells were co-stimulated with *E. coli* LPS (100 ng ml^{-1}) at 4 hpi. **(E)** BepD domain architecture of *B. henselae* strain Houston-1. 18 tyrosine (Y) residues embedded in conserved EPIYA-related tyrosine phosphorylation motifs are sequentially numbered from Y1' to Y9' or Y1 to Y9 within the two almost identical pY' (blue) and pY (orange) domains, respectively. The C-terminal BID domain represents the signal for T4SS-mediated protein translocation. **(F)** Direct comparison of the EPIYA-related motifs conserved in BepD orthologs (red; connected by blue or orange lines for motifs of pY' or pY, respectively). Phosphotyrosine motifs with no clear relationship to those present in *B. henselae* are shown in grey. A full protein sequence comparison of the presented BepD orthologs is shown in **Figure S2A. (G)** Graphical overview of a protein sequence alignment comparing the pY' and pY domains of *B. henselae* Houston-1 BepD with the ortholog of *B. henselae* strains A242 that comprises only a single pY domain. All nine EPIYA-related tyrosine phosphorylation motifs (Backert and Selbach, 2005) are identical in the three aligned pY domains and highlighted as sequence logos. **(H)** JAWS II cells were infected at MOI=100 with *B. henselae* wild-type, the Bep-deficient mutant *ΔbepA-G*, or *ΔbepA-G* derivatives expressing *B. henselae* BepD full-length (p*bepD*),

N-terminal truncated $BepD_t$ lacking pY' (p*bepD$_t$*), or $BepD_{BID}$ lacking pY' and pY thus expressing only the BID domain (p*bepD$_{BID}$*). Cells were co-stimulated with *E. coli* LPS (100 ng ml^{-1}) at 4 hpi. At 6 hpi, secreted TNF-α was quantified by ELISA. **(I)** Left panel: Expression of GFP (negative control) or GFP-$BepD_t$ wt (wild-type sequence) were induced with doxycycline (1 µg ml^{-1}) for 24 h, followed by 2 h stimulation with *E. coli* LPS (100 ng ml^{-1}) or mock treatment; right panel: Expression of GFP-$BepD_t$ wt, the indicated single Y-to-F exchange mutants, and the quintuple mutant GFP-$BepD_t$ 5Ymut were induced with doxycycline (1 µg ml^{-1}) for 24 h, followed by 2 h stimulation with *E. coli* LPS (100 ng ml^{-1}). TNF-α in culture supernatants was quantified by ELISA. Mean ± SD of triplicate data from one representative experiment (n = 3) are presented. Data were analyzed by one-way ANOVA followed by unpaired t-test. *P ≤ 0.05; **P < 0.01; P*** < 0.001; ns = non-significant.

Figure 2. Tyrosine-phosphorylation of the BepD pY domain leads to recruitment and phosphorylation of STAT3 on Y_{705}.

(A) Expression of GFP-$BepD_t$ wt or GFP-$BepD_t$ 5Ymut in JAWS II cells was induced by addition of doxycycline (1 µg ml^{-1}) for 24 h. A GFP-pulldown was performed and specific interaction partners were identified by mass spectrometry. Volcano plot representing significance (q-values) versus the GFP-$BepD_t$ wt / GFP-$BepD_t$ 5Ymut interaction ratio of indicated interaction partners on the y- and x-axes, respectively. Interactions with a q-value < 0.01 were considered significantly different between the two conditions and are highlighted in red. Underlined proteins harbor an SH2 domain. **(B)** A phosphoproteomics experiment was performed with the same cell lines and under identical assay conditions. Volcano plot representing significance (q-values) versus the GFP-$BepD_t$ wt / GFP-$BepD_t$ 5Ymut phosphorylation ratio on the y- and x-axes, respectively. Phosphopeptides with a q-value < 0.01 were considered significantly different between the two conditions and are highlighted in red. **(C)** Graphical representation of the interactome and phosphoproteome using STRING (Szklarczyk et al., 2019) (high confidence 0.7). Only proteins with at least one connection in STRING are represented. Hits from the interactome are colored in blue and hits from the phosphoproteome in green. STAT3 highlighted in orange was the only hit that was found significant in both interactor and phosphoprotein analysis. **(D)** GFP-$BepD_t$ wt or GFP-$BepD_t$ 5Ymut expression was induced in JAWS II cells by addition of doxycycline (1 µg ml^{-1}) for 24 h. A GFP-pulldown with cell lysates was performed and the input, flow through and pulldown fractions were analyzed by immunoblot with specific antibodies against GFP, p-STAT3 (Y_{705}), STAT3, or p-Tyr. (E) Expression of GFP-$BepD_t$ or indicated Y-to-F-exchange mutants in cell lysates of samples shown in Fig. 1I (right panel). Presented is an immunoblot probed with specific antibodies for p-STAT3 (Y_{705}) and GFP. Actin was used as loading control. Data from one representative experiment (n = 3) are presented.

Figure 3. BepD triggers STAT3 phosphorylation by a JAK-independent but c-Abl-dependent pathway.

(A) p-STAT3 dimerizes and translocates to the nucleus where it promotes transcription of multiple genes controlling cell growth, cell survival and inflammation, including down-regulation of TNF-α secretion. Ruxolitinib inhibits JAK-dependent STAT3 phosphorylation, whereas imatinib blocks c-Abl-dependent STAT3 phosphorylation. **(B)** Expression of GFP-$BepD_t$ wt (wt) or GFP-$BepD_t$ 5Ymut (5Ymut) in JAWS II cells was induced by addition of doxycycline (1 µg ml^{-1}) for 24 h. Cells were either left untreated or treated with 5 µM ruxolitinib for 1 h, followed by stimulation with LPS (100 ng ml^{-1}) for additional 4 h. Cells were harvested, lysed and analyzed by immunoblot with a specific p-STAT3 (Y_{705}) antibody. Actin was used as loading control. As positive control, JAWS II cells expressing GFP were treated with ruxolitinib and then stimulated with IL-6 (20 ng ml^{-1}) to induce canonical STAT3 activation via JAK. **(C)** TNF-α secreted by cells analyzed in (B) was quantified by ELISA. **(D)** Expression of GFP-$BepD_t$ wt (wt) or GFP-$BepD_t$ 5Ymut (5Ymut) in JAWS II cells was induced by addition of doxycycline (1 µg ml^{-1}) for 24 h. Cells were either left untreated or treated with 10 µM imatinib for 2 h, followed by cell harvest, lysis and use of ell lysates for a GFP-pulldown. Lysates before (input) and after pulldown (flow through) the pulldown fractions were analyzed by immunoblot with antibodies directed against GFP, p-STAT3 (Y_{705}), STAT3 and phospho-tyrosine (p-Tyr). The position of GFP-$BepD_t$. **(E)** Expression of GFP-$BepD_t$ (wt) or GFP-$BepD_t$ 5Ymut (5Ymut) in JAWS II cells was induced by addition of doxycycline (1 µg ml^{-1}) for 24 h. Cells were either left untreated or treated with 10 µM ruxolitinib for 1 h followed by stimulation with LPS (100 ng ml^{-1}) for 4 h. Cells were harvested, lysed and analyzed by immunoblot with a specific p-STAT3 (Y_{705}) antibody. Actin was used as loading control. **(F)** TNF-α secreted by cells analyzed in (E) was quantified by ELISA. Mean ± SD of triplicate data from one representative experiment (n = 3) are presented. Data were analyzed by one-way ANOVA followed by unpaired t-test. *P ≤ 0.05; **P < 0.01; P*** < 0.001.; ns = non-significant.

Figure 4. BepD triggers IL-10 secretion in *B. henselae*-infected macrophages

(A-D) RAW 264.7 macrophages or (**E, F**) bone marrow-derived macrophages (BMM) were infected at MOI=50 with *B. henselae* wild-type, the Bep-deficient mutant *ΔbepA-G* or its BepD-expressing derivative *ΔbepA-G* + p*bepD*. (**A**) At 6 hpi cells were harvested, lysed and analyzed by immunoblot for phospho-STAT3 (Y_{705}). Actin was used as loading control. **(B, E)** At 6 hpi secreted TNF-α was quantified by ELISA. (**D**) At indicated times (hpi) or (**C, F**) at 6 hpi secreted IL-10 was quantified by ELISA. Mean ± SD of triplicates from one representative experiment (n = 3) are presented. Data were analyzed by one-way ANOVA followed by unpaired t-test. *P ≤ 0.05; **P < 0.01; P*** < 0.001; P**** < 0.0001.

STAR METHODS

KEY RESOURCE TABLE

METHOD DETAILS

Bacterial strains, growth conditions and conjugations. All bacterial strains used in this study are listed in the Key Resources Table.

E. coli strains were cultivated in lysogeny broth (LB) or on solid agar plates (LA) supplemented with appropriate antibiotics at 37 °C overnight.

Plasmids were introduced into *Bartonella* strains by conjugation from *E. coli* strain β2150 using three-parental mating (Dehio and Meyer, 1997). When indicated, antibiotics or supplements were used in the following concentrations: kanamycin at 30 µg ml^{-1}, gentamicin at 10 µg ml^{-1}, streptomycin at 100 µg ml^{-1}, isopropyl-β-D-thiogalactoside (IPTG) at 100 µM and diaminopimelic acid (DAP) at 1 mM.

Bartonella strains were grown at 35 °C and 5% CO_2 on Columbia blood base agar (CBA) plates supplemented with 5% defibrinated sheep blood (CBA blood agar plate) and appropriate antibiotics. In general, *Bartonella* strains stored as frozen stocks at -80°C were inoculated as “thumbnails” on CBA blood agar plates for 3 days and subsequently expanded on fresh CBA blood agar plates for 2 days. Prior to infection *Bartonella* strains were cultured in M199 medium supplemented with 10% fetal calf serum (FCS) for 24 h at 35°C and 5% CO_2 in order to induce expression of the VirB/VirD4/Bep system (Quebatte et al., 2013).

Construction of strains and plasmids. DNA manipulations were performed according to standard techniques and all cloned inserts were DNA sequenced to confirm sequence integrity. For protein complementation/overexpression in *B. henselae* selected genes were cloned into plasmid pPG100 under the control of the *taclac* promoter (Schulein and Dehio, 2002). For protein overexpression in JAWS II cells, genes of interest were placed under control of the TET-inducible promoter pTF (Giry-Laterriere et al., 2011) by cloning into the lenti vector plasmid pCLX-pTF-R1-DEST-R2-EBR65 using standard gateway cloning strategy (Gateway system, Invitrogen). TET-modified pTF promoter was induced by adding

doxycycline to a final concentration of 1 µg ml^{-1}. A detailed description for the construction of each plasmid is presented in Table S3. The sequence of all oligonucleotide primers used in this study is listed in Table S4.

Cell lines and culture conditions. JAWS II cell line is a GM-CSF-dependent DC line established from bone marrow cells of a p53-knockout C57BL/6 mouse (Jiang et al., 2008b). JAWS II cells were cultured at 37°C in 5% CO_2 in complete culture medium consisting of MDM with 20% FCS, 4 mM L-glutamine, 1 mM sodium pyruvate and 5 ng ml^{-1} GM-CSF.

RAW 264.7 cell line is a murine macrophage cell line originating from an adult male BALB/c mouse (Raschke et al., 1978). RAW 264.7 cells were cultured at 37°C and 5% CO2 in DMEM Glutamax supplemented with 10% FCS.

Primary dendritic cells (DCs) were isolated from the spleens of C57BL/6 mice. Briefly, spleens were taken out and digested in RPMI 1640 containing 2% FCS and 3 mg ml^{-1} collagenase IV for 30 to 60 min at 37°C. To perform DC isolation, the Pan Dendritic Cell Isolation kit was used according to the manufacturer's recommendations.

Primary bone marrow-derived macrophages were derived from C57BL/6 mice and cultivated as described elsewhere (Figueira et al., 2013). In brief, cells were extracted from tibias and femurs. Erythrocytes were lysed in 0.83% NH_4Cl and remaining bone marrow cells were seeded at a density of 1.5 $x10^6$ cells/dish in complete medium consisting of DMEM supplemented with 1 mM Na-pyruvate, 10% FCS, 0.01 M HEPES, 0.005 mM β-ME, 100 U mL^{-1} Pen/Strep and 20% L929-cell (kindly provided by S. Helaine) conditioned medium at 5% CO_2 and 37°C. After 3 days, culture was supplemented with fresh complete medium. On day 7 cells were washed and $1x10^6$ cells/well seeded in complete medium without antibiotics in 12-well plates. Cells were incubated overnight before infection.

Cell infections. *B. henselae* strains were cultured as described above. One day before infection, $1×10^5$ cells (JAWS II, RAW 264.7), $2×10^5$ cells (splenic DCs) or $1x10^6$ cells (bone marrow-derived macrophages) were seeded per well in 12-well plates if not indicated

otherwise. Next day, cells were washed once with infection medium (DMEM Glutamax, supplemented with 1% FCS) and infected with a multiplicity of infection (MOI) of 50 bacteria per cell in infection medium supplemented with 100 µM IPTG (to induce protein expression in bacteria if required). Bacterial attachment was synchronized by centrifugation at 500 *g* for 3 min. Infected cells were incubated at 37°C and 5% CO_2 for indicated time periods. If indicated, cells were stimulated at 4 hpi. with 100 ng ml^{-1} LPS and incubated for additional 2 h at 37°C and 5% CO_2. Supernatants were analyzed by Ready-SET-Go! ELISA kits for TNF-α and IL-10. Adherent cells were harvested, lysed and analyzed by immunoblot.

Lentiviral transduction of JAWS II cells. To generate stable cell lines with integrated transgenes of interest, lentiviral transduction was performed as previously described (Okujava et al., 2014). In brief, 3×10^6 HEK 293T cells were seeded in a 10 cm cell-culture dish and transfected with a total of 5 µg of plasmid DNA following the FuGENE transfection protocol (FuGENE® 6 Transfection Reagent). After 6 h, the cell culture media was exchanged with fresh medium. For viral production, the cells were kept in culture for additional 48 h. One day before the viral transduction 5×10^4 JAWS II were seeded per well in a 6-well plate. The viral supernatant was collected, filtered through a 0.45 µm filter and 3 ml of viral supernatant was transferred onto JAWS II cells and 0.5 µg ml^{-1} Polybrene was added to each well. After 6 h, the cell culture medium was replaced by complete culture medium for JAWS II cells. Two days after transduction, selection with 5 µg ml^{-1} blasticidin was performed for additional 7 days to enrich transduced JAWS II cells.

Quantification of cytokine levels in culture supernatants. TNF-α and IL-10 were quantified in cell culture supernatants of infected cells by mouse specific sandwich ELISA according to the manufacturer's instructions. Absolute concentrations were measured using a standard curve provided by the manufacturer.

Immunoblot analysis. SDS-PAGE and immunoblotting were performed as described (Schulein et al., 2005). To verify expression levels of the protein of interest, JAWS II or RAW 264.7 cells were collected and washed twice with 2 ml ice-cold PBS. Cell pellets were lysed by adding 100 µl lysed with Novagen`s PhosphoSafe™ extraction buffer complemented with cOmplete™ Mini EDTA-free protease inhibitor cocktail. Protein concentrations of the cleared lysates were quantified using the Pierce™ BCA Protein Assay kit. Lysates with equal protein concentrations were mixed with Laemmli sample buffer, and resolved on 4 – 20% precast protein TGX gels. Pre-stained Precision Plus Protein™ Dual Color Standard was used as protein size reference. Proteins were transferred onto Amersham™ Protran® Nitocellulose Blotting membrane. Immunoblotting was performed using specific antibodies directed against the protein of interest followed by detection with horseradish peroxidase-conjugated antibodies directed against rabbit or mouse IgG. In all experiments, immunoblots were developed using LumiGLO® chemiluminescent substrate and imaged using an ImageQuant LAS 4000 device (GE Healthcare). If required blots were quantified using ImageJ.

GFP-Trap®_A for Immunoprecipitation. 24 hours after seeding lentiviral-transduced JAWS II cells, the expression of GFP-fused BepD constructs was induced by the addition of 1 µg ml^{-1} doxycycline for additional 24 h. Cells were harvested on ice, washed twice with ice-cold PBS and incubated with lysis buffer (10 mM Tris-HCl pH 7.5, 150 mM NaCl, 0.5 mM EDTA, 0.5% NP-40, 1x PhosSTOP™, cOmplete™ Mini EDTA-free protease inhibitor cocktail for 30 minutes on ice. Cell lysates were cleared by 20'000 x *g* centrifugation at 4 °C for 30 min. Supernatants were transferred to a new tube and subsequently diluted with 1.5 amounts of dilution buffer (10 mM Tris-HCl pH 7.5, 150 mM NaCl, 0.5 mM EDTA). A sample of the diluted lysates was taken as input sample. The remaining diluted cell lysates were then added to GFP-Trap® Agarose beads equilibrated in dilution buffer and incubated for 1 hour at 4 °C tumbled end-over end. After incubation supernatants were removed and kept as unbound fractions, beads were washed four times with ice-cold dilution buffer.

When analyzed by immunoblot, beads were resuspended in 2x SDS-sample buffer (120 mM Tris-HCl pH 6.8; 20% glycerol; 4% SDS, 0.04% bromophenol blue; 10% β-mercaptoethanol) and incubated 10 min at 95°C to dissociate immunocomplexes from GFP-Trap® Agarose beads. For analysis by mass spectrometry beads were eluted 3 times with ice-cold 0.2 M glycine pH 2.5. The eluate was neutralized with ammonium bicarbonate to pH 8, then urea was added to a final concentration of 1.6 M.

Preparation of immunoprecipitated samples for mass spectrometry. Disulfide bonds were reduced with tris (2-carboxyethyl) phosphine with a final concentration of 10 mM at 37°C for 1 h. Free thiols were alkylated with 20 mM iodoacetamide at room temperature for 30 min in the dark. The excess of iodoacetamide was quenched with final concentration of 25 mM N-acetyl-L-cysteine for 10 min at room temperature. The proteins were digested overnight at 37°C with sequencing-grade modified trypsin at a protein-to-enzyme ratio of 50:1. Peptides were desalted on a C18 Sep-Pak cartridge (Waters) and dried under vacuum.

Sample preparation for phosphoproteomics. 24 h after seeding JAWS II cells, expression of GFP-fused BepD constructs was induced by addition of 1 µg ml^{-1} doxycycline for further 24 h. Then plates were put on ice and washed twice with ice-cold PBS, followed by collection of samples in urea solution (8 M urea, 0.1 M ammonium bicarbonate, 1× PhosSTOP™). The samples were briefly vortexed, sonicated at 4°C, shaked for 5 min at room temperature and centrifuged for 20 min at 4°C and 16'000 *g*. Supernatants were collected and stored at -80°C for further processing. The Pierce™ BCA Protein Assay kit was used to measure protein concentration.

Phosphopeptide enrichment. Disulfide bonds were reduced with tris (2-carboxyethyl) phosphine at a final concentration of 10 mM at 37°C for 1 h. Free thiols were alkylated with 20 mM iodoacetamide at room temperature for 30 min in the dark. The excess of iodoacetamide was quenched with N-acetyl-L-cysteine at a final concentration of 25 mM for

10 min at room temperature. Lys-C endopeptidase was added to a final enzyme/protein ratio of 1:200 (w/w) and incubated for 4 h at 37°C. The solution was subsequently diluted with 0.1 M ammonium bicarbonate to a final concentration below 2 M urea and digested overnight at 37°C with sequencing-grade modified trypsin at a protein-to-enzyme ratio of 50:1. Peptides were desalted on a C18 Sep-Pak cartridge and dried under vacuum. Phosphopeptides were isolated from 2 mg of total peptide mass with TiO_2 as described previously (Schmutz et al., 2013). Briefly, dried peptides were dissolved in an 80% acetonitrile (I)–2.5% trifluoroacetic acid (TFA) solution saturated with phthalic acid. Peptides were added to the same amount of equilibrated TiO_2 (5-µm bead size, GL Sciences) in a blocked Mobicol spin column that was incubated for 30 min with end-over-end rotation. The column was washed twice with the saturated phthalic acid solution, twice with 80% ACN and 0.1% TFA, and finally twice with 0.1% TFA. The peptides were eluted with a 0.3 M ammonium hydroxide solution. The pH of the eluates was adjusted to be below 2.5 with 5% TFA solution and 2 M hydrochloride acid. Phosphopeptides were again desalted with microspin C18 cartridges.

LC-MS/MS analysis. Chromatographic separation of peptides was carried out using an EASY nano-LC system (Thermo Fisher Scientific), equipped with a heated 30 cm RP-HPLC column (75 µm x 45 cm) packed in-house with 1.9 µm C18 resin (Reprosil-AQ Pur, Dr.Maisch). Phosphopeptide samples were analyzed per LC-MS/MS run using a linear gradient ranging from 98% solvent A (0.15% formic acid) and 2% solvent B (98% acetonitrile, 2% water, 0.15% formic acid) to 30% solvent B over 120 min at a flow rate of 200 nl min^{-1}. Peptides derived from immunoprecipitation experiments were analyzed separated on a 60 min gradient. Mass spectrometry analysis was performed on a dual pressure LTQ-Orbitrap mass spectrometer equipped with a nano-electrospray ion source (both Thermo Fisher Scientific). Each MS1 scan (acquired with the Orbitrap) was followed by collision-induced dissociation (CID, acquired in the LTQ) of the 10 most abundant precursor ions with dynamic exclusion for 30 s. For phosphopeptide analysis, the 10 most abundant precursor ions were subjected to CID with enabled multistage activation. Total cycle time was approximately 2 s.

For MS1, 106 ions were accumulated in the Orbitrap cell over a maximum time of 300 ms and scanned at a resolution of 240'000 FWHM (at 400 m z^{-1}). MS2 scans were acquired using the rapid scan mode, a target setting of 104 ions, and accumulation time of 25 ms. Single charged ions and ions with unassigned charge state were excluded from triggering MS2 events. The normalized collision energy was set to 35%, and one microscan was acquired for each spectrum.

Label-free Quantification and Database Searching. The acquired raw-files were imported into the Progenesis software tool (Nonlinear Dynamics) for label-free quantification using the default parameters. MS2 spectra were exported directly from Progenesis in mgf format and searched using the MASCOT algorithm (Matrix Science) against a decoy database containing normal and reverse sequences of the predicted SwissProt entries of *Mus musculus* (www.ebi.ac.uk) and commonly observed contaminants generated using the Sequence Reverser tool from the MaxQuant software. The precursor ion tolerance was set to 10 ppm and fragment ion tolerance was set to 0.6 Da. The search criteria were set as follows: full tryptic specificity was required (cleavage after lysine or arginine residues unless followed by proline), 2 missed cleavages were allowed, carbamidomethylatiI (C) was set as fixed modification and phosphorylation (S, T, Y) or oxidation (M) as a variable modification for TiO_2 enriched or not enriched samples, respectively. Finally, the database search results were exported as a xml-file and imported back to the Progenesis software for MS1 feature assignment. For phosphopeptide quantification, a csv-file containing the MS1 peak abundances of all detected features was exported and for not enriched samples, a csv-file containing all protein measurements based on the summed feature intensities of all identified peptides per protein was created. Importantly, the Progenesis software was set that proteins identified by similar sets of peptides are grouped together and that only non-conflicting peptides with specific sequences for single proteins in the database were employed for protein quantification. Both files were further processed using the in-house developed SafeQuant R script (https://github.com/eahrne/SafeQuant). In brief, the software sets the

identification level False Discovery Rate to 1% (based on the number of decoy protein sequence database hits) and normalizes the identified MS1 peak abundances (extracted ion chromatogram, XIC) across all samples, i.e. the summed XIC of all confidently identified peptide features is scaled to be equal for all LC-MS runs. In the case of the IP experiments, the summed XIC confidently identified peptide features, matching the bait proteins, were used for normalization. In the case of phosphoproteomics, all quantified phosphopeptides/proteins are assigned an abundance ratio for each time point, based on the median XIC per time point. The statistical significance of each ratio is given by its q-value (false discovery rate adjusted p values), obtained by calculating modified t-statistic p values and adjusting for multiple testing. The location of the phosphorylated residues was automatically assigned by MASCOT (score >10).

Identification of BepD orthologs in *Bartonella* genomes. Candidates for a comprehensive set of BepD orthologs were identified based on BepD of *B. henselae* Houston-1 by tBLASTn searches using BLAST implemented in Geneious Prime 2019.2.1 against the non-redundant NCBI sequence database. The BID domain and adjacent C-terminal end of well-studied *B. henselae* Houston-1 BepD were used as the query sequence, because this part of the effector is thought to act primarily as a bipartite secretion signal (Engel et al., 2011; Harms et al., 2017; Schulein et al., 2005). Incomplete sequences were excluded as well as identical duplicates with the exception of important model species *B. henselae*, *B. birtlesii*, and *B. tribocorum* where all representatives were included in the analysis. A set of 39 candidate BepD orthologs were recovered with several proteins annotated as BepH being the next best BLAST hits based on bit-score and sequence identity. All candidates were identified as true BepD orthologs by forming a closed group as sister clade of BepH in phylogenetic analyses as shown previously (Engel et al., 2011). BepD sequences from the following *Bartonella* strains were used in this analysis (protein accession in brackets): *Bartonella alsatica* IBS382 (J0Q110); *Bartonella birtlesii* IBS325 (UPI00036FD8B1); *B. birtlesii* E4 (UPI00036FD8B1); *B. birtlesii* E11 (UPI00036FD8B1); *B. birtlesii* H12 (UPI00031744FA); *B. birtlesii* LL-WM9

(J0PP81); *Bartonella doshiae* NCTC12862 (A0A380ZGK7); *Bartonella elizabethae* F9251 (J1K3Z1); *Bartonella grahamii* as4aup (C6AES8); *B. grahamii* ATCC700132 (C6AES8); *B. henselae* Houston-1 (Q5QT02); *B. henselae* A71 (Q5QT02); *B. henselae* JK50 (Q5QT02); *B. henselae* JK51 (Q5QT02); *B. henselae* F1 (Q5QT02); *B. henselae* U4 (I3QKE3); *B. henselae* A112 (I3QKE3); *B. henselae* A121 (I3QKE3); *B. henselae* A233 (I3QKE3); *B. henselae* BM1374165 (I3QKE3); *B. henselae* A20 UPI0004378F5A; *B. henselae* A74 (UPI00095C7F10); *B. henselae* A76 (UPI00095C7F10); *B. henselae* A235 (UPI00095F5DE2); *B. henselae* A242 (UPI00096499B3); *B. henselae* A244 (UPI00096499B3); *B. henselae* BM1374163 (UPI0004378F5A); *B. henselae* BM1374164 (UPI0004378F5A); *B. henselae* Zeus (UPI0003DF9732); *B. henselae* JK41 (UPI0003DF9732); *B. henselae* JK42 (UPI0003DF9732); *B. henselae* JK53 (UPI0003DF9732); *Bartonella taylorii* IBS296 (UPI00026E5F08); *B. taylorii* 8TBB (J1K5A2); *Bartonella tribocorum* L103 (A0A2M6USB1); *B. tribocorum* CIP105476 (A9IWP9); *B. tribocorum* BM1374166 (A9IWP9); *Bartonella vinsonii* spp. *berkhoffii* Winnie (N6UQF1); *Bartonella washoensis* 08-0475 (EJF86807).

Protein sequence alignments. Protein sequences were aligned using ClustalW and MAFFT implemented in Geneious Prime 2019.2.1 using standard settings and then manually curated. Sequence logos and coloring according to amino acid similarity at given positions (based on the Blosum62 score matrix) were added using the respective functions in Geneious Prime 2019.2.1. 100% similarity is highlighted in green, 80-100% and 60-80% similarity in dark and light yellow, respectively, and <60% similarity without coloring.

Ethics statement. Animals were handled in strict accordance with good animal practice as defined by the relevant European (European standards of welfare for animals in research), national (Information and guidelines for animal experiments and alternative methods, Federal Veterinary Office of Switzerland) and/or local animal welfare bodies. Animal work was approved by the Veterinary Office of the Canton Basel City on June 2003 (license no. 1741).

Statistical analysis. Graphs were generated with GraphPad Prism 8. Statistical analyses were performed using one-way ANOVA followed by unpaired Student's t test..For the graphs presented in the figures, significance was denoted as non-significant (ns) ($P > 0.05$); * $P \leq 0.05$; ** $P < 0.01$; *** $P < 0.001$; P**** < 0.0001.

Data availability

The data that support the findings of this study are available from the corresponding authors on reasonable request.

704 **REFERENCES**

705 Aderem, A., and Ulevitch, R.J. (2000). Toll-like receptors in the induction of the innate
706 immune response. Nature *406*, 782-787.

707 Allen, J.C., Talab, F., Zuzel, M., Lin, K., and Slupsky, J.R. (2011). c-Abl regulates Mcl-1 gene
708 expression in chronic lymphocytic leukemia cells. Blood *117*, 2414-2422.

709 Backert, S., and Selbach, M. (2005). Tyrosine-phosphorylated bacterial effector proteins: the
710 enemies within. Trends Microbiol *13*, 476-484.

711 Bermond, D., Heller, R., Barrat, F., Delacour, G., Dehio, C., Alliot, A., Monteil, H., Chomel,
712 B., Boulouis, H.J., and Piemont, Y. (2000). Bartonella birtlesii sp. nov., isolated from
713 small mammals (Apodemus spp.). Int J Syst Evol Microbiol *50 Pt 6*, 1973-1979.

714 Dehio, C., and Meyer, M. (1997). Maintenance of broad-host-range incompatibility group P
715 and group Q plasmids and transposition of Tn5 in *Bartonella henselae* following
716 conjugal plasmid transfer from *Escherichia coli*. J Bacteriol *179*, 538-540.

717 Druker, B.J., Talpaz, M., Resta, D.J., Peng, B., Buchdunger, E., Ford, J.M., Lydon, N.B.,
718 Kantarjian, H., Capdeville, R., Ohno-Jones, S.*, et al.* (2001). Efficacy and safety of a
719 specific inhibitor of the BCR-ABL tyrosine kinase in chronic myeloid leukemia. N Engl J
720 Med *344*, 1031-1037.

721 Engel, P., Salzburger, W., Liesch, M., Chang, C.C., Maruyama, S., Lanz, C., Calteau, A.,
722 Lajus, A., Medigue, C., Schuster, S.C.*, et al.* (2011). Parallel evolution of a type IV
723 secretion system in radiating lineages of the host-restricted bacterial pathogen
724 *Bartonella*. PLoS Genet *7*, e1001296.

725 Figueira, R., Watson, K.G., Holden, D.W., and Helaine, S. (2013). Identification of salmonella
726 pathogenicity island-2 type III secretion system effectors involved in intramacrophage
727 replication of *S. enterica* serovar typhimurium: implications for rational vaccine design.
728 MBio *4*, e00065.

729 Garcia, R., Bowman, T.L., Niu, G.L., Yu, H., Minton, S., Muro-Cacho, C.A., Cox, C.E.,
730 Falcone, R., Fairclough, R., Parsons, S.*, et al.* (2001). Constitutive activation of Stat3

731 by the Src and JAK tyrosine kinases participates in growth regulation of human breast
732 carcinoma cells. Oncogene *20*, 2499-2513.
733 Giry-Laterriere, M., Cherpin, O., Kim, Y.S., Jensen, J., and Salmon, P. (2011). Polyswitch
734 lentivectors: "all-in-one" lentiviral vectors for drug-inducible gene expression, live
735 selection, and recombination cloning. Hum Gene Ther *22*, 1255-1267.
736 Guindon, S., Dufayard, J.F., Lefort, V., Anisimova, M., Hordijk, W., and Gascuel, O. (2010).
737 New algorithms and methods to estimate maximum-likelihood phylogenies: assessing
738 the performance of PhyML 3.0. Syst Biol *59*, 307-321.
739 Guye, P. (2005). Proteins injected by the bacterial pathogen "*Bartonella*" subvert eukaryotic
740 cell signaling. In Biozentrum (edoc of University of Basel: University of Basel),
741 https://edoc.unibas.ch/739/, pp. 91-93.
742 Hannemann, S., Gao, B.L., and Galan, J.E. (2013). *Salmonella* Modulation of Host Cell Gene
743 Expression Promotes Its Intracellular Growth. Plos Pathogens *9*.
744 Harms, A., and Dehio, C. (2012). Intruders below the Radar: Molecular Pathogenesis of
745 *Bartonella* spp. Clin Microbiol Rev *25*, 42-78.
746 Harms, A., Segers, F.H.I.D., Quebatte, M., Mistl, C., Manfredi, P., Korner, J., Chomel, B.B.,
747 Kosoy, M., Maruyama, S., Engel, P.*, et al.* (2017). Evolutionary Dynamics of
748 Pathoadaptation Revealed by Three Independent Acquisitions of the VirB/D4 Type IV
749 Secretion System in *Bartonella*. Genome Biol Evol *9*, 761-776.
750 Harrison, C., and Vannucchi, A.M. (2012). Ruxolitinib: a potent and selective Janus kinase 1
751 and 2 inhibitor in patients with myelofibrosis. An update for clinicians. Ther Adv
752 Hematol *3*, 341-354.
753 Hayashi, T., Morohashi, H., and Hatakeyama, M. (2013). Bacterial EPIYA effectors--where
754 do they come from? What are they? Where are they going? Cell Microbiol *15*, 377-385.
755 Hillmer, E.J., Zhang, H.Y., Li, H.S., and Watowich, S.S. (2016). STAT3 signaling in immunity.
756 Cytokine Growth F R *31*, 1-15.

Hobbs, S., Reynoso, M., Geddis, A.V., Mitrophanov, A.Y., and Matheny, R.W. (2018). LPS-stimulated NF-kappa B p65 dynamic response marks the initiation of TNF expression and transition to IL-10 expression in RAW 264.7 macrophages. Physiol Rep *6*.

Hong, J., Li, Y., Hua, X., Bai, Y., Wang, C., Zhu, C., Du, Y., Yang, Z., and Yuan, C. (2017). Lymphatic Circulation Disseminates Bartonella Infection Into Bloodstream. J Infect Dis *215*, 303-311.

Jaslow, S.L., Gibbs, K.D., Fricke, W.F., Wang, L.Y., Pittman, K.J., Mammel, M.K., Thaden, J.T., Fowler, V.G., Hammer, G.E., Elfenbein, J.R.*, et al.* (2018). *Salmonella* Activation of STAT3 Signaling by SarA Effector Promotes Intracellular Replication and Production of IL-10. Cell Rep *23*, 3525-3536.

Jiang, X., Shen, C., Rey-Ladino, J., Yu, H., and Brunham, R.C. (2008a). Characterization of murine dendritic cell line JAWS II and primary bone marrow-derived dendritic cells in *Chlamydia muridarum* antigen presentation and induction of protective immunity. Infect Immun *76*, 2392-2401.

Jiang, X.Z., Shen, C.X., Rey-Ladino, J., Yu, H., and Brunham, R.C. (2008b). Characterization of murine dendritic cell line JAWS II and primary bone marrow-derived dendritic cells in *Chlamydia muridarum* antigen presentation and induction of protective immunity. Infection and Immunity *76*, 2392-2401.

Katoh, K., Rozewicki, J., and Yamada, K.D. (2019). MAFFT online service: multiple sequence alignment, interactive sequence choice and visualization. Brief Bioinform *20*, 1160-1166.

Koenig, T., Menze, B.H., Kirchner, M., Monigatti, F., Parker, K.C., Patterson, T., Steen, J.J., Hamprecht, F.A., and Steen, H. (2008). Robust prediction of the MASCOT score for an improved quality assessment in mass spectrometric proteomics. J Proteome Res *7*, 3708-3717.

Koesling, J., Aebischer, T., Falch, C., Schulein, R., and Dehio, C. (2001). Cutting edge: antibody-mediated cessation of hemotropic infection by the intraerythrocytic mouse pathogen Bartonella grahamii. J Immunol *167*, 11-14.

McGinnis, S., and Madden, T.L. (2004). BLAST: at the core of a powerful and diverse set of sequence analysis tools. Nucleic Acids Res *32*, W20-25.

Menheniott, T.R., Judd, L.M., and Giraud, A.S. (2015). STAT3: a critical component in the response to *Helicobacter pylori* infection. Cell Microbiol *17*, 1570-1582.

Mogensen, T.H. (2009). Pathogen Recognition and Inflammatory Signaling in Innate Immune Defenses. Clin Microbiol Rev *22*, 240-+.

Murray, P.J. (2007). The JAK-STAT signaling pathway: Input and output intergration. J Immunol *178*, 2623-2629.

Murray, P.J., Allen, J.E., Biswas, S.K., Fisher, E.A., Gilroy, D.W., Goerdt, S., Gordon, S., Hamilton, J.A., Ivashkiv, L.B., Lawrence, T.*, et al.* (2014). Macrophage Activation and Polarization: Nomenclature and Experimental Guidelines (vol 41, pg 14, 2014). Immunity *41*, 339-340.

Okujava, R., Guye, P., Lu, Y.Y., Mistl, C., Polus, F., Vayssier-Taussat, M., Halin, C., Rolink, A.G., and Dehio, C. (2014). A translocated effector required for *Bartonella* dissemination from derma to blood safeguards migratory host cells from damage by co-translocated effectors. PLoS Pathog *10*, e1004187.

Quebatte, M., Dick, M.S., Kaever, V., Schmidt, A., and Dehio, C. (2013). Dual input control: activation of the Bartonella henselae VirB/D4 type IV secretion system by the stringent sigma factor RpoH1 and the BatR/BatS two-component system. Mol Microbiol *90*, 756-775.

Raschke, W.C., Baird, S., Ralph, P., and Nakoinz, I. (1978). Functional Macrophage Cell Lines Transformed by Abelson Leukemia-Virus. Cell *15*, 261-267.

Rhomberg, T.A., Truttmann, M.C., Guye, P., Ellner, Y., and Dehio, C. (2009). A translocated protein of Bartonella henselae interferes with endocytic uptake of individual bacteria and triggers uptake of large bacterial aggregates via the invasome. Cell Microbiol *11*, 927-945.

Rizzuti, D., Ang, M., Sokollik, C., Wu, T., Abdullah, M., Greenfield, L., Fattouh, R., Reardon, C., Tang, M., Diao, J.*, et al.* (2015). *Helicobacter pylori* inhibits dendritic cell maturation

via interleukin-10-mediated activation of the signal transducer and activator of transcription 3 pathway. J Innate Immun *7*, 199-211.

Safari, F., Murata-Kamiya, N., Saito, Y., and Hatakeyama, M. (2011). Mammalian Pragmin regulates Src family kinases via the Glu-Pro-Ile-Tyr-Ala (EPIYA) motif that is exploited by bacterial effectors. P Natl Acad Sci USA *108*, 14938-14943.

Schmid, M.C., Scheidegger, F., Dehio, M., Balmelle-Devaux, N., Schulein, R., Guye, P., Chennakesava, C.S., Biedermann, B., and Dehio, C. (2006). A translocated bacterial protein protects vascular endothelial cells from apoptosis. PLoS Pathog *2*, e115.

Schmid, M.C., Schulein, R., Dehio, M., Denecker, G., Carena, I., and Dehio, C. (2004). The VirB type IV secretion system of *Bartonella henselae* mediates invasion, proinflammatory activation and antiapoptotic protection of endothelial cells. Mol Microbiol *52*, 81-92.

Schmutz, C., Ahrne, E., Kasper, C.A., Tschon, T., Sorg, I., Dreier, R.F., Schmidt, A., and Arrieumerlou, C. (2013). Systems-level overview of host protein phosphorylation during *Shigella flexneri* infection revealed by phosphoproteomics. Mol Cell Proteomics *12*, 2952-2968.

Schneider, C.A., Rasband, W.S., and Eliceiri, K.W. (2012). NIH Image to ImageJ: 25 years of image analysis. Nat Methods *9*, 671-675.

Schulein, R., and Dehio, C. (2002). The VirB/VirD4 type IV secretion system of *Bartonella* is essential for establishing intraerythrocytic infection. Mol Microbiol *46*, 1053-1067.

Schulein, R., Guye, P., Rhomberg, T.A., Schmid, M.C., Schroder, G., Vergunst, A.C., Carena, I., and Dehio, C. (2005). A bipartite signal mediates the transfer of type IV secretion substrates of *Bartonella henselae* into human cells. P Natl Acad Sci USA *102*, 856-861.

Selbach, M., Paul, F.E., Brandt, S., Guye, P., Daumke, O., Backert, S., Dehio, C., and Mann, M. (2009). Host cell interactome of tyrosine-phosphorylated bacterial proteins. Cell Host Microbe *5*, 397-403.

840 Suarez, A.A.R., Van Renne, N., Baumert, T.F., and Lupberger, J. (2018). Viral manipulation
841 of STAT3: Evade, exploit, and injure. Plos Pathogens *14*.
842 Szklarczyk, D., Gable, A.L., Lyon, D., Junge, A., Wyder, S., Huerta-Cepas, J., Simonovic, M.,
843 Doncheva, N.T., Morris, J.H., Bork, P.*, et al.* (2019). STRING v11: protein-protein
844 association networks with increased coverage, supporting functional discovery in
845 genome-wide experimental datasets. Nucleic Acids Res *47*, D607-D613.
846 The UniProt, C. (2017). UniProt: the universal protein knowledgebase. Nucleic Acids Res *45*,
847 D158-D169.
848 Vermi, W., Facchetti, F., Riboldi, E., Heine, H., Scutera, S., Stornello, S., Ravarino, D.,
849 Cappello, P., Giovarelli, M., Badolato, R.*, et al.* (2006). Role of dendritic cell-derived
850 CXCL13 in the pathogenesis of *Bartonella henselae* B-rich granuloma. Blood *107*, 454-
851 462.
852 Wagner, A., and Dehio, C. (2019). Role of distinct type-IV-secretion systems and secreted
853 effector sets in host adaptation by pathogenic *Bartonella* species. Cell Microbiol *21*.
854 Wen, Z., Zhong, Z., and Darnell, J.E., Jr. (1995). Maximal activation of transcription by Stat1
855 and Stat3 requires both tyrosine and serine phosphorylation. Cell *82*, 241-250.
856 Xu, S., Zhang, C., Miao, Y., Gao, J., and Xu, D. (2010). Effector prediction in host-pathogen
857 interaction based on a Markov model of a ubiquitous EPIYA motif. BMC Genomics *11*
858 *Suppl 3*, S1.
859 Yu, H., Pardoll, D., and Jove, R. (2009). STATs in cancer inflammation and immunity: a
860 leading role for STAT3. Nat Rev Cancer *9*, 798-809.
861 Zahringer, U., Lindner, B., Knirel, Y.A., van den Akker, W.M., Hiestand, R., Heine, H., and
862 Dehio, C. (2004). Structure and biological activity of the short-chain lipopolysaccharide
863 from *Bartonella henselae* ATCC 49882T. J Biol Chem *279*, 21046-21054.

864

Figure 1

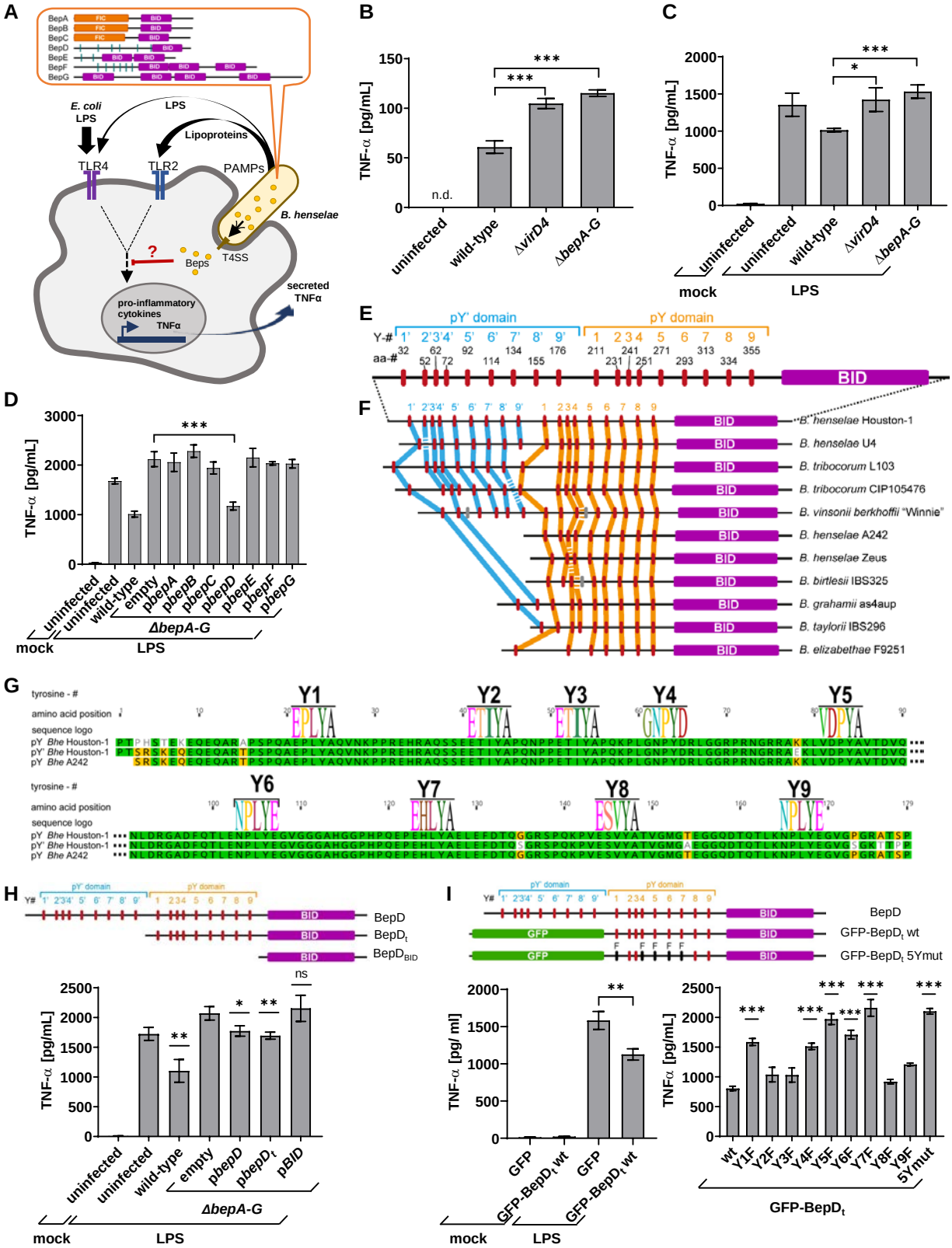
A
BepA
BepB
BepC
BepD
BepE
BepF
BepG
FIC
BID
E. coli LPS
LPS
Lipoproteins
TLR4
TLR2
PAMPs
B. henselae
?
Beps
T4SS
pro-inflammatory cytokines
TNFα
secreted TNFα
B
TNF-α [pg/mL]
n.d.
***
uninfected
wild-type
ΔvirD4
ΔbepA-G
C
TNF-α [pg/mL]
***
*
uninfected
uninfected
wild-type
ΔvirD4
ΔbepA-G
mock
LPS
D
TNF-α [pg/mL]
***
uninfected
uninfected
wild-type
empty
pbepA
pbepB
pbepC
pbepD
pbepE
pbepF
pbepG
ΔbepA-G
mock
LPS
E
pY' domain
pY domain
Y-#
aa-#
BID
F
B. henselae Houston-1
B. henselae U4
B. tribocorum L103
B. tribocorum CIP105476
B. vinsonii berkhoffii "Winnie"
B. henselae A242
B. henselae Zeus
B. birtlesii IBS325
B. grahamii as4aup
B. taylorii IBS296
B. elizabethae F9251
G
tyrosine - #
amino acid position
sequence logo
Y1
Y2
Y3
Y4
Y5
Y6
Y7
Y8
Y9
pY Bhe Houston-1
pY Bhe Houston-1
pY Bhe A242
H
BepD
BepDt
BepDBID
TNF-α [pg/mL]
ns
**
*
**
uninfected
uninfected
wild-type
empty
pbepD
pbepDt
pBID
ΔbepA-G
mock
LPS
I
BepD
GFP-BepDt wt
GFP-BepDt 5Ymut
TNF-α [pg/ ml]
**
GFP
GFP-BepDt wt
GFP
GFP-BepDt wt
mock
LPS
TNFα [pg/mL]
***
wt
Y1F
Y2F
Y3F
Y4F
Y5F
Y6F
Y7F
Y8F
Y9F
5Ymut
GFP-BepDt

Figure 2

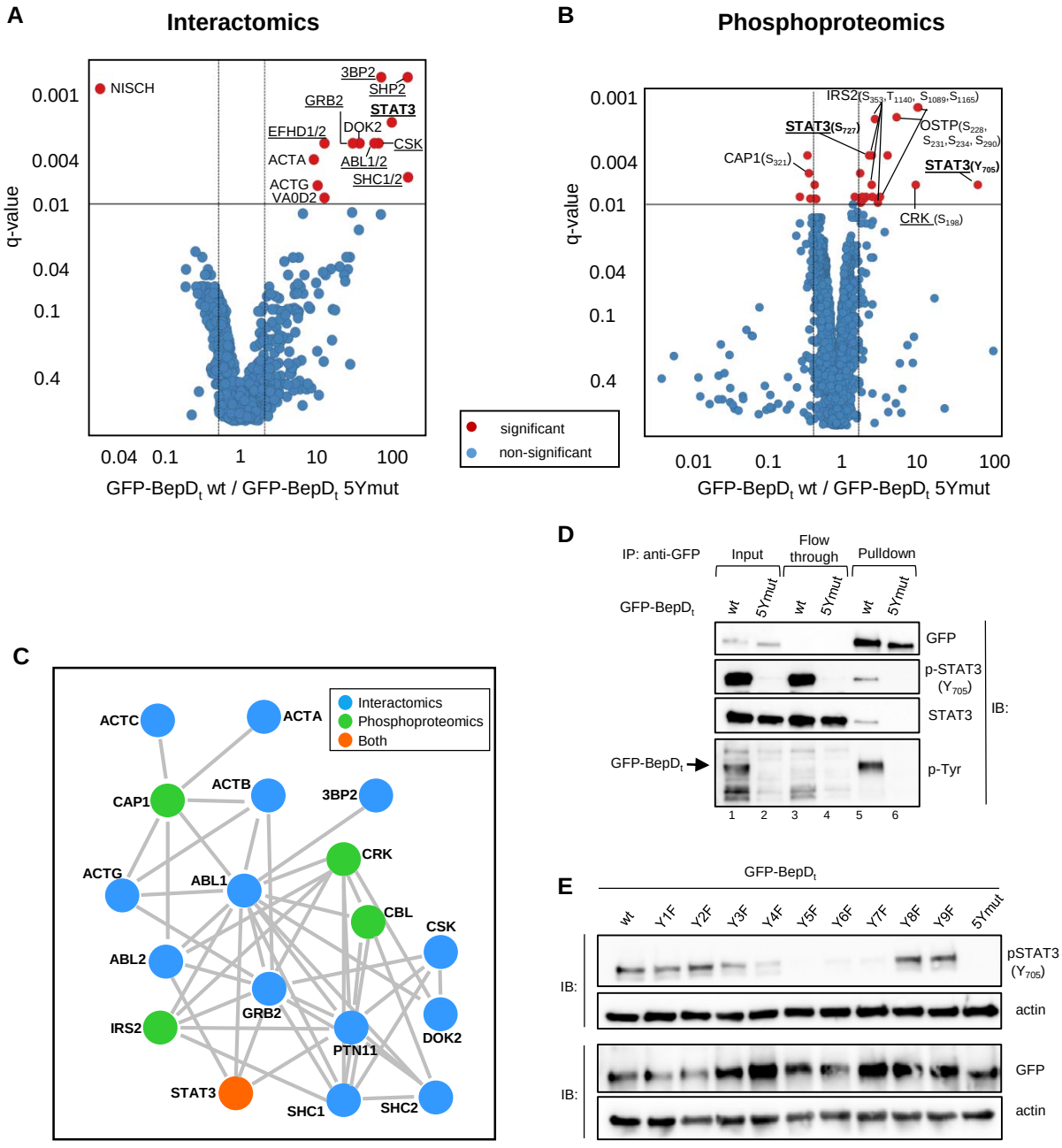
A
Interactomics
NISCH
3BP2
SHP2
GRB2
STAT3
EFHD1/2
DOK2
CSK
ACTA
ABL1/2
ACTG
VA0D2
SHC1/2
0.001
0.004
0.01
0.04
0.1
0.4
q-value
0.04 0.1 1 10 100
GFP-BepD$_t$ wt / GFP-BepD$_t$ 5Ymut
significant
non-significant
B
Phosphoproteomics
IRS2(S$_{353}$,T$_{1140}$, S$_{1089}$,S$_{1165}$)
STAT3(S$_{727}$)
OSTP(S$_{228}$, S$_{231}$,S$_{234}$, S$_{290}$)
CAP1(S$_{321}$)
STAT3(Y$_{705}$)
CRK (S$_{198}$)
0.001
0.004
0.01
0.04
0.1
0.4
q-value
0.01 0.1 1 10 100
GFP-BepD$_t$ wt / GFP-BepD$_t$ 5Ymut
C
Interactomics
Phosphoproteomics
Both
ACTC
ACTA
ACTB
CAP1
3BP2
CRK
ACTG
ABL1
CBL
CSK
ABL2
GRB2
IRS2
DOK2
PTN11
STAT3
SHC1
SHC2
D
IP: anti-GFP
Input
Flow through
Pulldown
GFP-BepD$_t$
wt
5Ymut
GFP
p-STAT3 (Y$_{705}$)
STAT3
p-Tyr
IB:
1 2 3 4 5 6
E
GFP-BepD$_t$
wt
Y1F
Y2F
Y3F
Y4F
Y5F
Y6F
Y7F
Y8F
Y9F
5Ymut
IB:
pSTAT3 (Y$_{705}$)
actin
GFP
actin

Figure 3

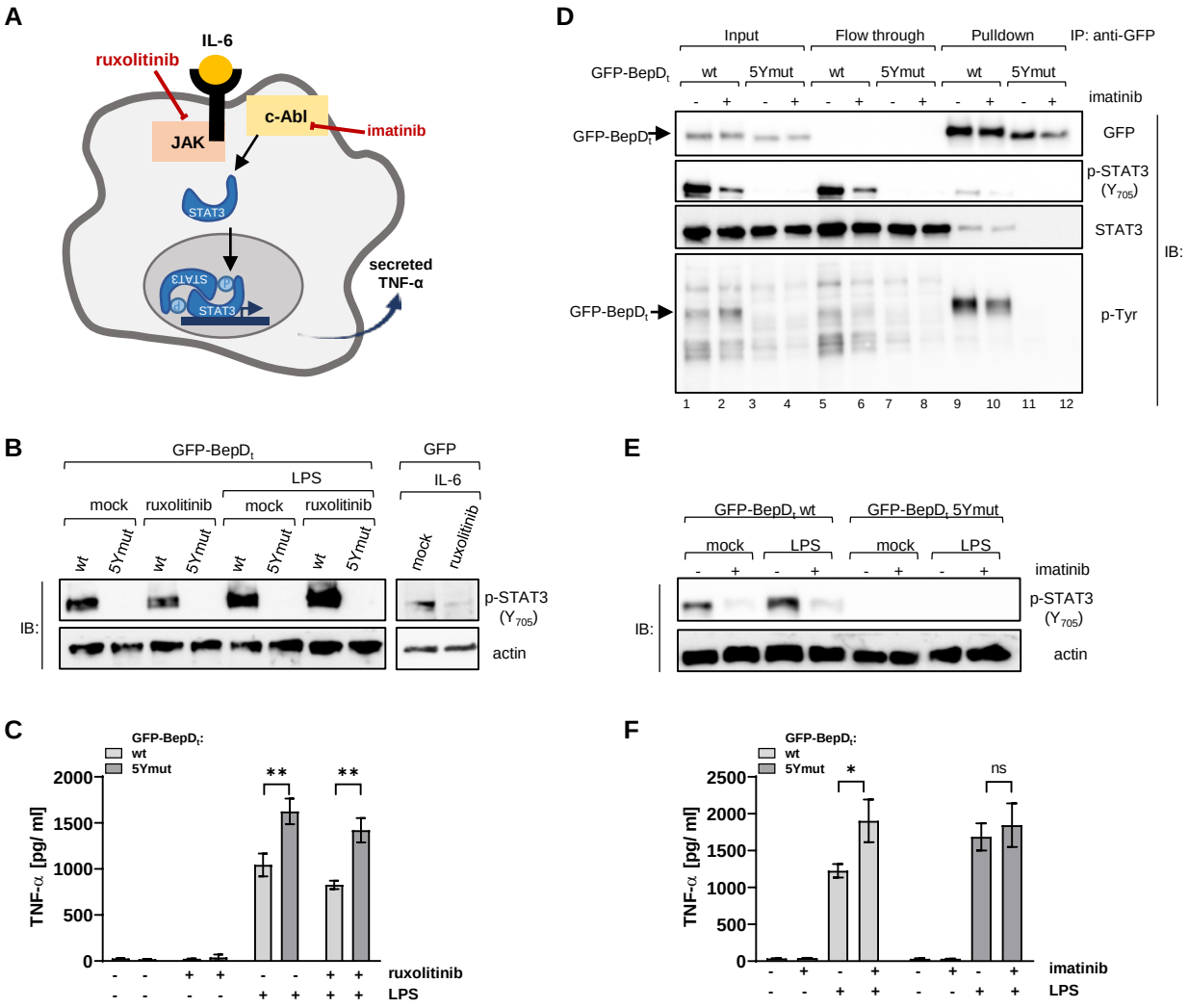
A
IL-6
ruxolitinib
JAK
c-Abl
imatinib
STAT3
secreted
TNF-α
D
Input
Flow through
Pulldown
IP: anti-GFP
GFP-BepD$_t$
wt
5Ymut
imatinib
GFP
p-STAT3 (Y$_{705}$)
STAT3
p-Tyr
IB:
1 2 3 4 5 6 7 8 9 10 11 12
B
GFP-BepD$_t$
GFP
LPS
IL-6
mock
ruxolitinib
p-STAT3 (Y$_{705}$)
actin
E
GFP-BepD$_t$ wt
GFP-BepD$_t$ 5Ymut
C
GFP-BepD$_t$:
TNF-α [pg/ ml]
ruxolitinib
LPS
F
ns
imatinib

Figure 4

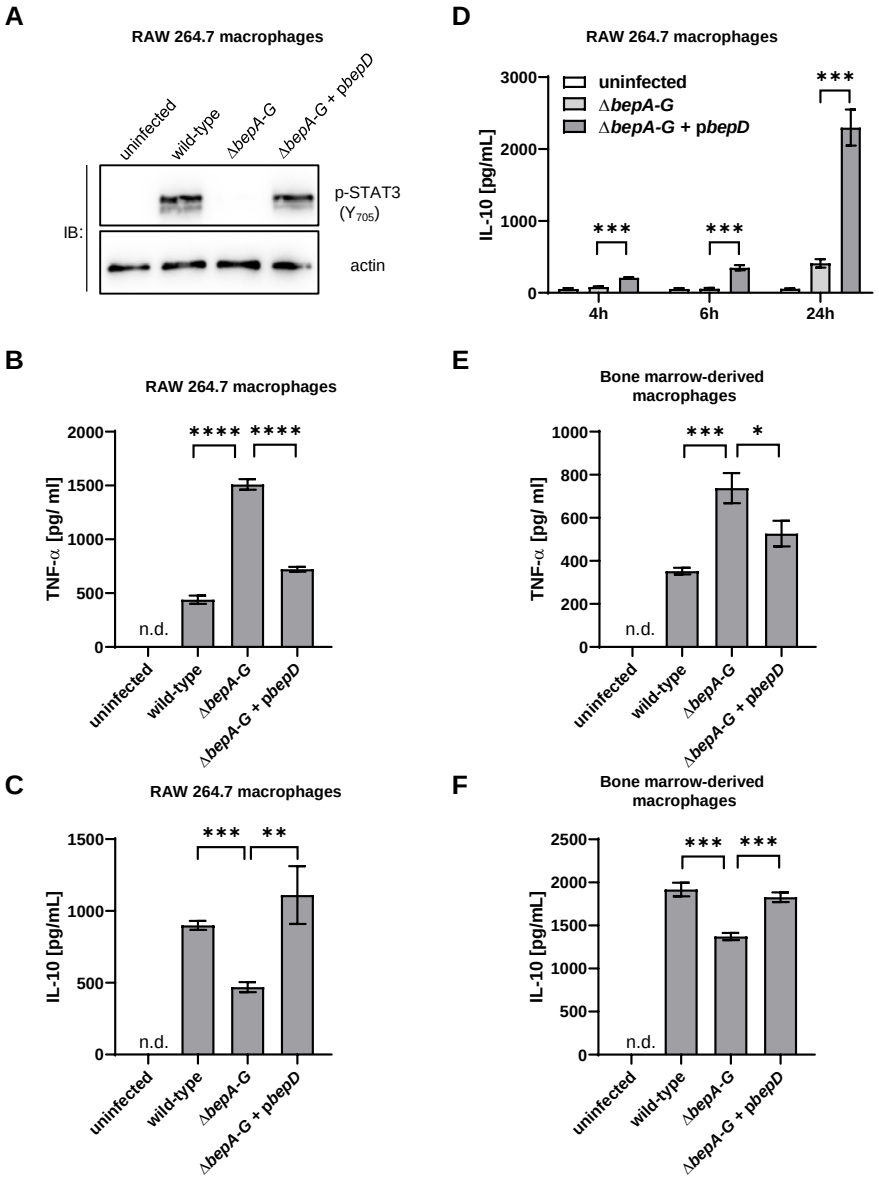
A
RAW 264.7 macrophages
uninfected
wild-type
ΔbepA-G
ΔbepA-G + pbepD
IB:
p-STAT3 (Y705)
actin
D
RAW 264.7 macrophages
uninfected
ΔbepA-G
ΔbepA-G + pbepD
IL-10 [pg/mL]
3000
2000
1000
0
***
***
***
4h
6h
24h
B
RAW 264.7 macrophages
TNF-α [pg/ ml]
2000
1500
1000
500
0
****
****
n.d.
uninfected
wild-type
ΔbepA-G
ΔbepA-G + pbepD
E
Bone marrow-derived macrophages
TNF-α [pg/ ml]
1000
800
600
400
200
0
***
*
n.d.
uninfected
wild-type
ΔbepA-G
ΔbepA-G + pbepD
C
RAW 264.7 macrophages
IL-10 [pg/mL]
1500
1000
500
0
***
**
n.d.
uninfected
wild-type
ΔbepA-G
ΔbepA-G + pbepD
F
Bone marrow-derived macrophages
IL-10 [pg/mL]
2500
2000
1500
1000
500
0
***
***
n.d.
uninfected
wild-type
ΔbepA-G
ΔbepA-G + pbepD

SUPPLEMENTAL INFORMATION

Figure S1 (Related to Figure 1)

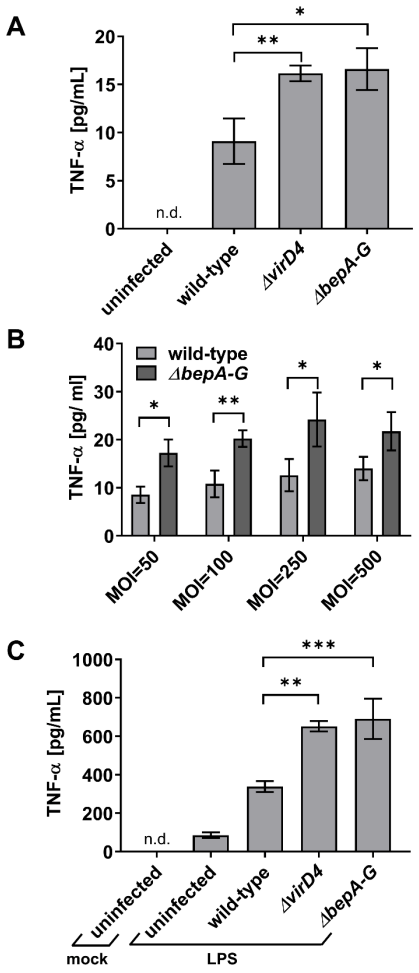

Figure S1: TNF-α secretion of mouse splenic dendritic cells upon infection with *B. henselae*

(A) Mouse splenic DCs were infected for 6 h with either *B. henselae* wild-type, the Type-VI-secretion-deficient mutant *ΔvirD4*, or the Bep-deficient mutant *ΔbepA-G* at a multiplicity of infection (MOI) of 25, followed by quantification of TNF-α in culture supernatants by ELISA. **(B)** Mouse splenic DCs were infected as described in (A) but with different MOI as indicated. **(C)** Mouse splenic DCs were infected with MOI 50 as described in (A) except for the addition of *E. coli* LPS (100 ng ml^{-1}) at 4 hpi. Data are displayed as the mean ± SD of a technical triplicate. The data were analyzed by one-way ANOVA followed by unpaired t-test.*P ≤ 0.05; **P < 0.01; P*** < 0.001; n.d. = not detectable.

Figure S2 (Related to Figure 1)

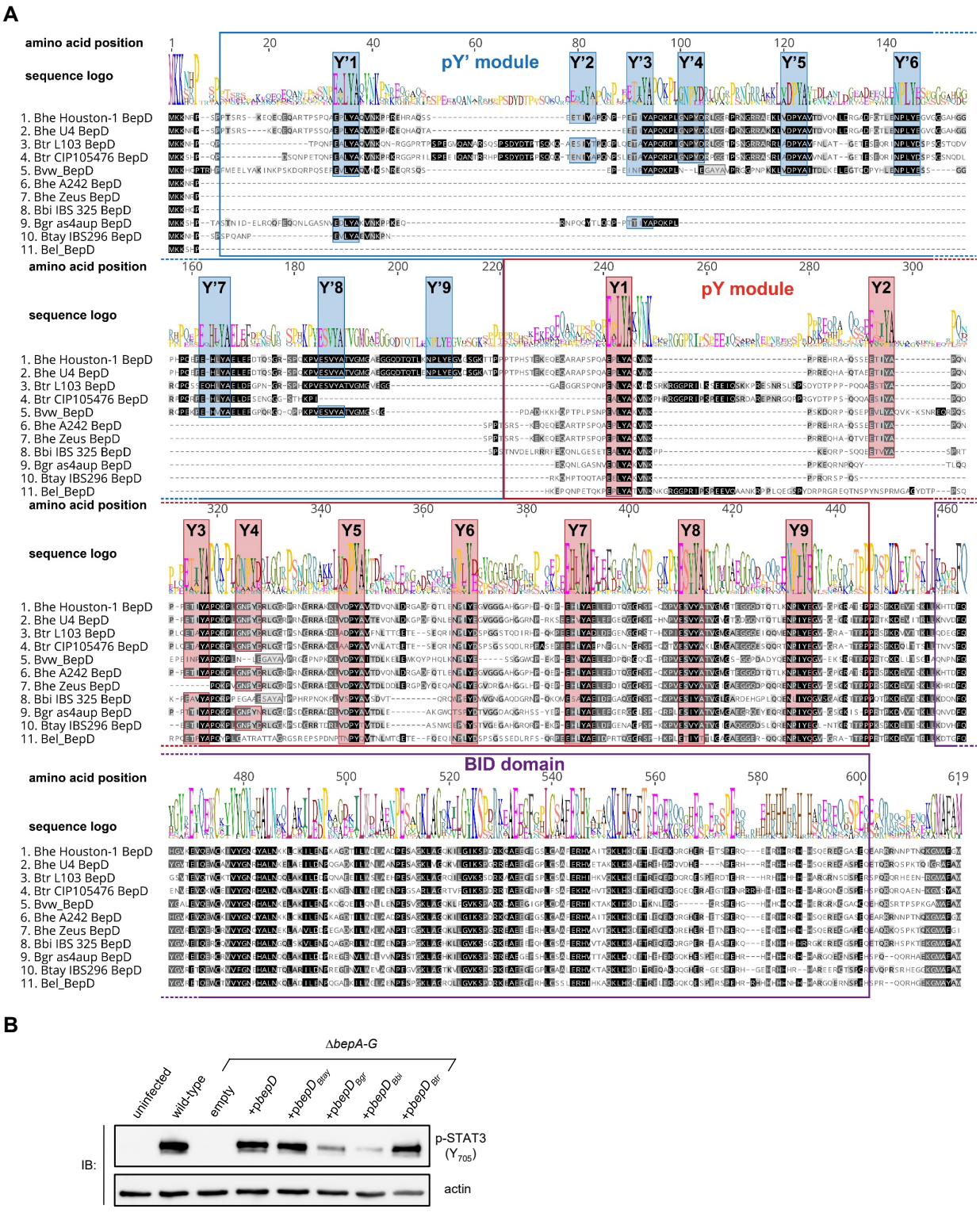

Figure S2: Comparison of BepD protein sequences and capacity of BepD orthologs from different *Bartonella* species to activate STAT3. (A) Sequence alignment of a subset of 11 BepD orthologs that are representatives of all identified patterns of phosphotyrosine

motif composition. Amino acids were highlighted in greyscale if all amino acids at a given position were 100% similar (black), 80-100% similar (dark grey), or 60-80% similar (light grey) based on the Blosum62 score matrix with a threshold value of 2. Phosphotyrosine motifs identified as belonging to the pY' module are highlighted in blue, those identified as belonging to the pY module are highlighted in red, and other tentative phosphotyrosine modules are highlighted in grey. (**B**) JAWS II cells were infected at MOI=50 with *B. henselae* wild-type (wild-type), a Bep-deficient *ΔbepA-G* mutant (*ΔbepA-G*) or derivatives of this strain expressing BepD of different *Bartonella* species from a plasmid. At 4 hpi cells were co-stimulated with 100 ng ml^{-1} LPS. At 6 hpi cells were harvested, lysed and analyzed for p-STAT3 (Y_{705}) by immunoblot. Actin was used as loading control. Plasmids for expression of BepD homologs from different *Bartonella* species are indicated as follows: *B. henselae (*p*bepD)*, *B. taylorii* (p$bepD_{Btay}$), *B. grahamii* (p$bepD_{Bgr}$), *B. birtlesii* (p$bepD_{Bbi}$), *B. tribocorum* (p$bepD_{Btr}$).

Figure S3 (Related to Figure 3)

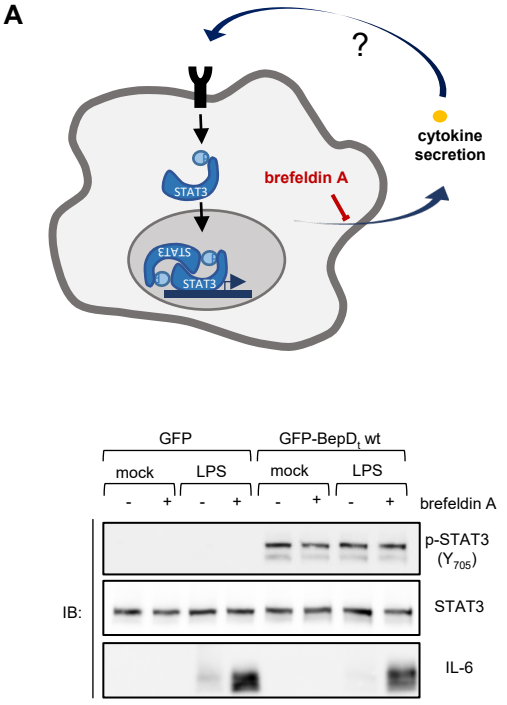

Figure S3: BepD-dependent STAT3 phosphorylation does not involve auto- or paracrine signaling but is dependent on the host kinase c-Abl. (**A**) JAWS II cells were treated with doxycycline (1 µg ml^{-1}) to induce expression of GFP or GFP-BepD$_t$ wt. Simultaneously brefeldin A (20 µg ml^{-1}) and LPS (100 ng ml^{-1}) were added for 7h. Phosphorylation of STAT3 on Y$_{705}$ was monitored by immunoblot. Total STAT3 serves as loading control. Intracellular IL-6 served as secretion inhibition control. Data from one representative experiment (n=3) are shown. (**B**) Signal intensities of relevant protein bands in Figure 3D lane 9 (mock) and lane 10 (imatinib) were quantified with ImageJ. Depicted are

arbitrary units for the respective bands given by the software. Indicated is the percentage of signal reduction in the imatinib treated sample compared to the mock control.

Figure S4 (Related to Figure 4)

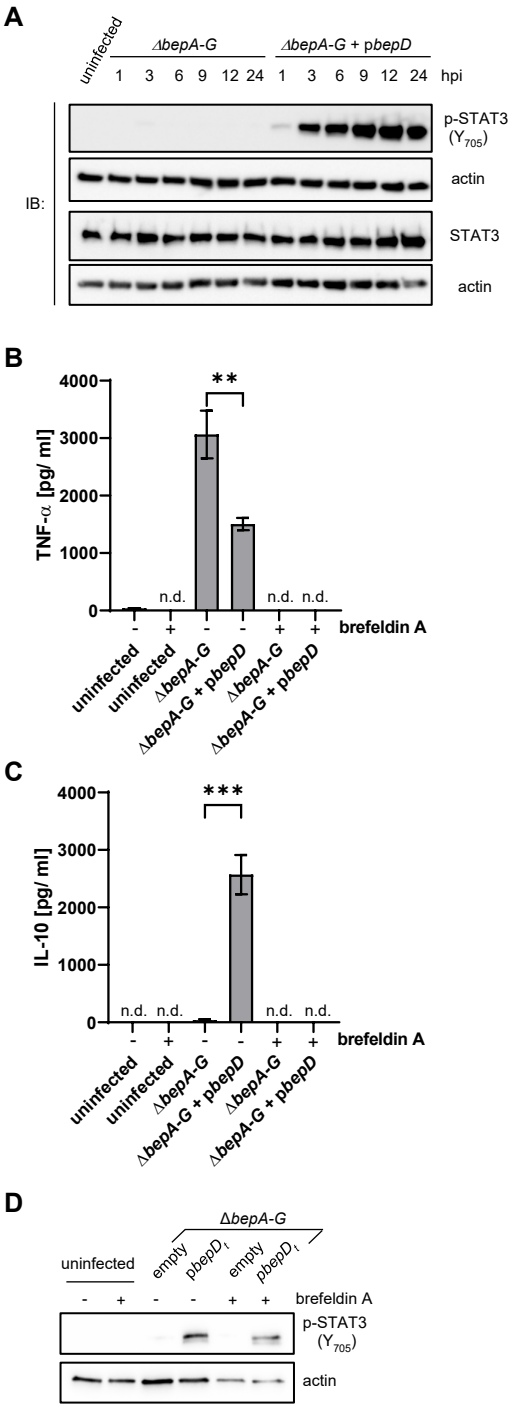

Figure S4: BepD-triggers sustained STAT3 phosphorylation in JAWS II cells and intrinsic STAT3 phosphorylation independent of auto- and paracrine signaling in RAW264.7 macrophages. (**A**) JAWS II cells were infected at MOI=50 with the *B. henselae*

Bep-deficient mutant *ΔbepA-G* or a derivate of this strain expressing *B. henselae* BepD from a plasmid (p*bepD*). At indicated timepoints cells were harvested and lysed. Cellular lysates were analyzed by immunoblot with specific antibodies for p-STAT3 (Y_{705}), STAT3, and actin. The actin signal was used as loading control. (**B**) RAW 264.7 macrophages ($5x10^5$ cells) were either treated with brefeldin A (5 µg ml^{-1}) or left untreated while infected at MOI=50 with *B. henselae* wild-type, the Bep-deficient mutant *ΔbepA-G* or its BepD-expressing derivative *ΔbepA-G* + p*bepD*. At 6 hpi secreted TNF-α and (**C**) IL-10 were quantified by ELISA. (**D**) Cells corresponding to panel (B and C) were harvested, lysed and analyzed by immunoblot for phospho-STAT3 (Y_{705}). Actin was used as loading control. Mean ± SD of triplicates from one representative experiment (n = 3) are presented. Data were analyzed by one-way ANOVA followed by unpaired t-test. *P ≤ 005; **P < 0.01; P*** < 0.001; n.d.= not detectable.

Table S1: List of peptides identified by phosphoproteomics (Related to Figure 2)

peptides	motifs	Accession	Description	Ratio GFP-BepD$_t$ wt / GFP-BepD$_t$ 5Ymut	q-value
YCRPESQEHPEADPGSAAPYLK	[20] Phospho (Y)	STAT3_MOUSE	Signal transducer and activator of transcription 3	77.77	0.007
LEHSKESQESADQSDVIDSQASSK	[4] Phospho (ST)|[7] Phospho (ST)	OSTP_MOUSE	Osteopontin	12.50	0.001
LEHSKESQESADQSDVIDSQASSK	[7] Phospho (ST)|[10] Phospho (ST)	OSTP_MOUSE	Osteopontin	12.30	0.001
YRPASASVSALIGGNQEGSHPQPLGGPEPGPYAQPSVNTPLPNLQNGPIYAR	[9] Phospho (ST)	CRK_MOUSE	Adapter molecule crk	11.61	0.007
ISHELESSSSEVN	[10] Phospho (ST)	OSTP_MOUSE	Osteopontin	6.48	0.002
IKPSSSANAIYSLAAR	[11] Phospho (Y)	CBL_MOUSE	E3 ubiquitin-protein ligase CBL	4.91	0.004
LEHSKESQESADQSDVIDSQASSK	[4] Phospho (ST)	OSTP_MOUSE	Osteopontin	3.88	0.009
RKQSESEIVPER	[6] Phospho (ST)	TBC14_MOUSE	TBC1 domain family member 14	3.64	0.010
VASPTSGLK	[3] Phospho (ST)	IRS2_MOUSE	Insulin receptor substrate 2	3.34	0.002
VEFGVYESGPR	[6] Phospho (Y) 694	BCAP_MOUSE	Phosphoinositide 3-kinase adapter protein 1	3.09	0.009
FICVTPTTCSNTIDLPMSPR	[18] Phospho (ST)	STAT3_MOUSE	Signal transducer and activator of transcription 3	3.03	0.004
RHNSASVENVSLR	[6] Phospho (ST)	IRS2_MOUSE	Insulin receptor substrate 2	3.00	0.007
HSSETFSSTTTVTPVSPSFAHNSK	[5] Phospho (ST)	IRS2_MOUSE	Insulin receptor substrate 2	2.78	0.004
EQEAKPSPEPAAGSR	[7] Phospho (ST)	ZN703_MOUSE	Zinc finger protein 703	2.52	0.009
SQSSGSSATHPISVPGAR	[3] Phospho (ST)	IRS2_MOUSE	Insulin receptor substrate 2	2.37	0.009
HTFGQKPSLSTEDSQEENTSK	[10] Phospho (ST)	FYB_MOUSE	FYN-binding protein	2.26	0.009
LGEQGPEPGPTPPQTPTPPSTPPLAK	[17] Phospho (ST)|[21] Phospho (ST)	RHG17_MOUSE	Rho GTPase-activating protein 17	2.16	0.010
RPGSVSSTDQER	[4] Phospho (ST)	I2BPL_MOUSE	Interferon regulatory factor 2-binding protein-like	2.12	0.005
RTGSNISGASSDVSLDEQYK	[7] Phospho (ST)	OSBP1_MOUSE	Oxysterol-binding protein 1	1.80	0.009
NRGSGGFGGGGTR	[4] Phospho (ST)	THOC4_MOUSE	THO complex subunit 4	0.55	0.009
SRHSPLLKSPFGK	[4] Phospho (ST)|[9] Phospho (ST)	KI20A_MOUSE	Kinesin-like protein KIF20A	0.55	0.009
ERDSELSDSDSGYGVGHSESDKSSTHGEGAAEADDK	[11] Phospho (ST)|[18] Phospho (ST)	UHRF1_MOUSE	E3 ubiquitin-protein ligase UHRF1	0.54	0.009
NHSPLSPPHPNHEEPSR	[3] Phospho (ST)|[6] Phospho (ST)	LCP2_MOUSE	Lymphocyte cytosolic protein 2	0.52	0.007
EHANIDAQSGSQAPNPSTTISPGKSPPPAK	[21] Phospho (ST)|[25] Phospho (ST)	SIR2_MOUSE	NAD-dependent protein deacetylase sirtuin-2	0.46	0.009
PFSAPKPQTSPSPKPATK	[10] Phospho (ST)|[12] Phospho (ST)	CAP1_MOUSE	Adenylyl cyclase-associated protein 1	0.44	0.005
SRSLSASPALGSTK	[3] Phospho (ST)|[7] Phospho (ST)	NADK_MOUSE	NAD kinase	0.42	0.004
ARPTSAGGLSLLPPPPGGK	[5] Phospho (ST)	NECP2_MOUSE	Adaptin ear-binding coat-associated protein 2	0.33	0.009

Table S2: List of peptides identified by interactomics (Related to Figure 2)

Accession	Description	# Peptides used for quantification	Ratio GFP-BepD$_t$ wt / GFP-BepD$_t$ 5Ymut	q-value	SH2 Domain
SHC1_MOUSE; SHC2_MOUSE	SHC-transforming protein 1	3	153.47	0.0057	✓
PTN11_MOUSE	Tyrosine-protein phosphatase non-receptor type 11	58	151.72	0.0007	✓
STAT3_MOUSE	Signal transducer and activator of transcription 3	53	94.25	0.0018	✓
3BP2_MOUSE	SH3 domain-binding protein 2	2	68.25	0.0007	✓
CSK_MOUSE	Tyrosine-protein kinase CSK	8	63.25	0.0028	✓
ABL2_MOUSE; ABL1_MOUSE	Abelson tyrosine-protein kinase 2	22	55.70	0.0028	✓
DOK2_MOUSE	Docking protein 2	14	35.66	0.0028	
GRB2_MOUSE	Growth factor receptor-bound protein 2	11	29.09	0.0028	✓
EFHD2_MOUSE; EFHD1_MOUSE	EF-hand domain-containing protein D2	6	12.35	0.0028	✓
VA0D2_MOUSE	V-type proton ATPase subunit d 2	3	12.34	0.0088	
CTB_MOUSE; ACTG_MOUSE	Actin, cytoplasmic 1	13	10.07	0.0068	
ACTC_MOUSE; ACTA_MOUSE	Actin, alpha cardiac muscle 1	3	8.99	0.0039	
NISCH_MOUSE	Nischarin	26	0.01	0.0009	

Table 3: List and construction of all plasmids used in this study (Related to STAR Methods)

Plasmid name	Description	internal designation	Primers used for insert PCR		Template for PCR	Details on molecular cloning			Source / Reference
			fwd	rev		restriction enzymes (insert)	vector backbone	restriction enzymes (vector)	
pPG100	*Bartonella* shuttle vector, encoding a FLAG epitope	pPG100							(Schulein et al., 2005)
p*bepA*	Derivative of pPG100, enconding FLAG::*Bhe* BepA	pPG101							(Schmid et al., 2006)
p*bepB*	Derivative of pPG100, encoding FLAG::*Bhe* BepB	pMS006							(Schmid et al., 2006)
p*bepC*	Derivative of pPG100, encoding FLAG::*Bhe* BepC	pMS007							(Schmid et al., 2006)
p*bepD*	Derivative of pPG100, encoding FLAG::*Bhe* BepD	pPG104							(Schulein et al., 2005)
p*bepE*	Derivative of pPG100, encoding FLAG::*Bhe* BepE	pPG105							(Rhomberg et al., 2009)
p*bepF*	Derivative of pPG100, encoding FLAG::*Bhe* BepF	pPG106							(Rhomberg et al., 2009)
p*bepG*	Derivative of pPG100, encoding FLAG::*Bhe* BepG	pPG107							(Rhomberg et al., 2009)
p$bepD_{BID}$	Derivative of pPG100, encoding FLAG::*Bhe* $BepD_{BID}$	pMS100-D							(Schmid et al., 2006)
p$bepD_t$	Derivative of pPG100, encoding FLAG::*Bhe* $BepD_t$	pLU030	prLU174	prLU175	boiled colony of *B. henselae* RSE 247	*Nde*I	pPG100	*Nde*I	this study
pLU044	Derivative of pPG100, encoding FLAG::*Bhe* $BepD_t$ 5Ymut (Y32/72/92/114/134F)	pLU044	prLU172 prLU183 prLU185 prLU252 prLU187 prLU189 prLU191 prLU160 prLU193	prLU173 prLU184 prLU186 prLU253 prLU188 prLU190 prLU192 prLU161 prLU194	pLU030	generated with site directed mutagenesis followed by *Dpn*I digest; after sequential mutation rounds $BepD_t$ 5Ymut fragment was cut and inserted into the parental pPG100 vector through *Nde*I ligation to avoid any further mutations			this study
p$bepD_{Btr}$	Derivative of pPG100, encoding FLAG::*Btr* BepD	pLU053	prLU265	prLU266	boiled colony of *B. tribocorum* RSE 149	*Nde*I	pPG100	*Nde*I	this study
p$bepD_{Bgr}$	Derivative of pPG100, encoding FLAG::*Bgr* BepD	pLU061	prLU281	prLU282	boiled colony of *B. grahamii* CDE142	*Nde*I	pPG100	*Nde*I	this study
p$bepD_{Bbi}$	Derivative of pPG100, encoding FLAG::*Bbi* BepD	pLU060	prLU234	prLU235	boiled colony of *B. birtlesii* PEE0249	*Nde*I	pPG100	*Nde*I	this study
p$bepD_{Bta}$	Derivative of pPG100, encoding FLAG::*Btay* BepD	pLU058	prLU074	prLU075	boiled colony of *B. taylorii* RSE 149	*Nde*I	pPG100	*Nde*I	this study
pRO300	pRRL-SV40(puro)_CMV(mcs), encoding eGFP	pRO300							(Okujava et al., 2014)
pLU073	pDONR-GFP, for gateway cloning	pLU073	prLU276	prLU277	pRO300	amplified PCR fragment was recombined to pDONR by gateway BP clonase reaction			this study
pLU074	pDONR-GFP-*Bhe* $BepD_t$ for gateway cloning	pLU074	a) prLU276 b) prLU199	a) prRO90 b) prLU278	a) pRO300 b) pLU030	Two PCR reactions were run to amplify a) GFP and b) *Bhe* $BepD_t$; in second SOEing PCR fragments were used with prLU276 and pr278; integrated into pDONR by two step gateway cloning			this study
pLU076	pDONR-Bhe BepD-BXBID 5Ymuts (Y32/72/92/114/134F), for gateway cloning	pLU076	a) prLU276 b) prLU199	a) prRO90 b) prLU278	a) pRO300 b) pLU044	Two PCR reactions were run to amplify a) GFP and b) *Bhe* $BepD_t$ 5Ymut; in a second SOEing PCR fragments were			this study

						used with prLU276 and prLU278; integrated into pDONR by two step gateway cloning	
pCS010	pDONR-Bhe BepD$_t$ Y32F	pCS010	prLU172	prLU173	pLU074	Site directed mutagenesis, followed by *Dpn*I digest of template yielding in the pDONR-entry plasmid	this study
pCS011	pDONR-Bhe BepD$_t$ Y52F	pCS011	prLU183	prLU184	pLU074	Site directed mutagenesis, followed by *Dpn*I digest of template yielding in the pDONR-entry plasmid	this study
pCS012	pDONR-Bhe BepD$_t$ Y62F	pCS012	prLU185	prLU186	pLU074	Site directed mutagenesis, followed by *Dpn*I digest of template yielding in the pDONR-entry plasmid	this study
pCS013	pDONR-Bhe BepD$_t$ Y72F	pCS013	prLU252	prLU253	pLU074	Site directed mutagenesis, followed by *Dpn*I digest of template yielding in the pDONR-entry plasmid	this study
pCS014	pDONR-Bhe BepD$_t$ Y92F	pCS014	prLU187	prLU188	pLU074	Site directed mutagenesis, followed by *Dpn*I digest of template yielding in the pDONR-entry plasmid	this study
pCS015	pDONR-Bhe BepD$_t$ Y114F	pCS015	prLU189	prLU190	pLU074	Site directed mutagenesis, followed by *Dpn*I digest of template yielding in the pDONR-entry plasmid	this study
pCS016	pDONR-Bhe BepD$_t$ Y134F	pCS016	prLU191	prLU192	pLU074	Site directed mutagenesis, followed by *Dpn*I digest of template yielding in the pDONR-entry plasmid	this study
pCS017	pDONR-Bhe BepD$_t$ Y155F	pCS017	prLU160	prLU161	pLU074	Site directed mutagenesis, followed by *Dpn*I digest of template yielding in the pDONR-entry plasmid	this study
pCS018	pDONR-Bhe BepD$_t$ Y176F	pCS018	prLU193	prLU194	pLU074	Site directed mutagenesis, followed by *Dpn*I digest of template yielding in the pDONR-entry plasmid	this study
GFP	pCLX, encoding GFP	pLU077			GFP fragment in pLU73 was recombined into the destination vector pCLX-pTF-R1-DEST-R2-EBR65 by gateway LR clonase reaction		this study
GFP-BepD$_t$	pCLX, encoding GFP::Bhe BepD$_t$	pLU078			GFP-BepD$_t$ fragment in pLU74 was recombined into the destination vector pCLX-pTF-R1-DEST-R2-EBR65 by gateway LR clonase reaction		this study
GFP-BepD$_t$ 5Ymut	pCLX, encoding GFP::Bhe BepD$_t$ 5Ymut	pLU080			GFP-BepD$_t$ 5Ymut fragment in pLU76 was recombined into the destination vector pCLX-pTF-R1-DEST-R2-EBR65 by gateway LR clonase reaction		this study
GFP-BepD$_t$ Y32F	pCLX, encoding GFP::Bhe BepD$_t$ Y32F	pCS019			GFP-BepD$_t$ Y32F fragment in pCS010 was recombined into the destination vector pCLX-pTF-R1-DEST-R2-EBR65 by gateway LR clonase reaction		this study
GFP-BepD$_t$ Y52F	pCLX, encoding GFP::Bhe BepD$_t$ Y52F	pCS020			GFP-BepD$_t$ Y52F fragment in pCS011 was recombined into the destination vector pCLX-pTF-R1-DEST-R2-EBR65 by gateway LR clonase reaction		this study
GFP-BepD$_t$ Y62F	pCLX, encoding GFP::Bhe BepD$_t$ Y62F	pCS021			GFP-BepD$_t$ Y62F fragment in pCS012 was recombined into the destination vector pCLX-pTF-R1-DEST-R2-EBR65 by gateway LR clonase reaction		this study
GFP-BepD$_t$ Y72F	pCLX, encoding GFP::Bhe BepD$_t$ Y72F	pCS022			GFP-BepD$_t$ Y72F fragment in pCS013 was recombined into the destination vector pCLX-pTF-R1-DEST-R2-EBR65 by gateway LR clonase reaction		this study
GFP-BepD$_t$ Y92F	pCLX, encoding GFP::Bhe BepD$_t$ Y92F	pCS023			GFP-BepD$_t$ Y92F fragment in pCS014 was recombined into the destination vector pCLX-pTF-R1-DEST-R2-EBR65 by gateway LR clonase reaction		this study
GFP-BepD$_t$ Y114F	pCLX, encoding GFP::Bhe BepD$_t$ Y114F	pCS024			GFP-BepD$_t$ Y114F fragment in pCS015 was recombined into the destination vector pCLX-pTF-R1-DEST-R2-EBR65 by gateway LR clonase reaction		this study
GFP-BepD$_t$ Y134F	pCLX, encoding GFP::Bhe BepD$_t$ Y134F	pCS025			GFP-BepD$_t$ Y134F fragment in pCS016 was recombined into the destination vector pCLX-pTF-R1-DEST-R2-EBR65 by gateway LR clonase reaction		this study
GFP-BepD$_t$ Y155F	pCLX, encoding GFP::Bhe BepD$_t$ Y155F	pCS026			GFP-BepD$_t$ Y155F fragment in pCS017 was recombined into the destination vector pCLX-pTF-R1-DEST-R2-EBR65 by gateway LR clonase reaction		this study
GFP-BepD$_t$ Y176F	pCLX, encoding GFP::Bhe BepD$_t$ Y176F	pCS027			GFP-BepD$_t$ Y176F fragment in pCS018 was recombined into the destination vector pCLX-pTF-R1-DEST-R2-EBR65 by gateway LR clonase reaction		this study
pMDL	packaging plasmid for viral production; expression of Gag-Pol	pMDL					(Okujava et al., 2014)
pREV	packaging plasmid for viral production; expression of REV	pREV					(Okujava et al., 2014)
pVSVG	packaging plasmid for viral production; expression of VSV-G	pVSVG					(Okujava et al., 2014)

Table S4: Oligonucleotides used in this study (Related to Table S3)

Cloning primers		
Name	**Sequence 5' - 3'**	**Restriction site**
prLU174	CGGCATATGTCAGGAAAGACAACACCCCCTCCGACA	*Nde*I
prLU175	CGGCATATGTTACATACCAAAGGCCATTCC	*Nde*I
prLU265	GGGAATTCCATATGCCAAAAGCCAAAGAA	*Nde*I
prLU266	GGGAATTCCATATGTTAGCTGGCTATAGCGAG	*Nde*I
prLU281	GGGAATTCCATATGAAAAAAAGTCACCCAACCGCT	*Nde*I
prLU282	GGGAATTCCATATGTTACATGGCAAAAGCCATTCC	*Nde*I
prLU74	CTTCATATGAAAAAGAATCATCCATCCCCTTCTC	*Nde*I
prLU75	AATCATATGTTACATCGCAAAAGCCATTCCTTTTCC	*Nde*I
prLU199	GGTGGCGGGCCCGGGATGTCAGGAAAGACA	
prLU276	GGGGACAAGTTTGTACAAAAAAGCAGGCTTCGAAGGAGATAGAACCATGGTGAGCAAGGGCGAGGAGCTG	
prLU277	GGGGACCACTTTGTACAAGAAAGCTGGGTCCTACTTGTACAGCTCGTCCATGC	
prLU278	GGGGACCACTTTGTACAAGAAAGCTGGGTCCTACATACCAAAGGCCATTCCTT	
prRO90	CCC GGG CCC GCC ACC CTT GTA CAG CTC GTC CAT GCC G	

Mutagenesis primer for tyrosine to phenylalanine exchanges		
Name	**Sequence 5' - 3'**	**Y to F**
prLU172	GCAGAACCCCTCTTTGCACAGGTAAAT	Y32F
prLU173	ATTTACCTGTGCAAAGAGGGGTTCTGC	Y32F
prLU183	AGAAGAAACTATCTTTGCACCTCAAAACC	Y52F
prLU184	GGTTTTGAGGTGCAAAGATAGTTTCTTCT	Y52F
prLU185	ACCAGAAACTATCTTTGCACCCCAAAAAC	Y62F
prLU186	GTTTTTGGGGTGCAAAGATAGTTTCTGGT	Y62F
prLU252	CCTCTAGGAAATCCCTTTGACAGACTTGGTGGG	Y72F
prLU253	CCCACCAAGTCTGTCAAAGGGATTTCCTAGAGG	Y72F
prLU187	ACTAGTAGACCCCTTTGCAGTAACTGATG	Y92F
prLU188	CATCAGTTACTGCAAAGGGGTCTACTAGT	Y92F
prLU189	AGAAAATCCCCTCTTTGAGGGAGTTGGCG	Y114F
prLU190	CGCCAACTCCCTCAAAGAGGGGATTTTCT	Y114F
prLU191	ACCAGAACATCTCTTTGCAGAGCTTGAAT	Y134F
prLU192	ATTCAAGCTCTGCAAAGAGATGTTCTGGT	Y134F
prLU160	TAGAATCTGTCTTTGCAACAGTTGGCA	Y155F
prLU161	TGCCAACTGTTGCAAAGACAGATTCTA	Y155F
prLU193	TAAAAAATCCCCTCTTCGAAGGAGTTGGCC	Y176F
prLU194	GGCCAACTCCTTCGAAGAGGGGATTTTTTA	Y176F

Supplement References:

Okujava, R., Guye, P., Lu, Y.Y., Mistl, C., Polus, F., Vayssier-Taussat, M., Halin, C., Rolink, A.G., and Dehio, C. (2014). A translocated effector required for *Bartonella* dissemination from derma to blood safeguards migratory host cells from damage by co-translocated effectors. PLoS Pathog *10*, e1004187.

Rhomberg, T.A., Truttmann, M.C., Guye, P., Ellner, Y., and Dehio, C. (2009). A translocated protein of *Bartonella henselae* interferes with endocytic uptake of individual bacteria and triggers uptake of large bacterial aggregates via the invasome. Cell Microbiol *11*, 927-945.

Schmid, M.C., Scheidegger, F., Dehio, M., Balmelle-Devaux, N., Schulein, R., Guye, P., Chennakesava, C.S., Biedermann, B., and Dehio, C. (2006). A translocated bacterial protein protects vascular endothelial cells from apoptosis. PLoS Pathog *2*, e115.

Schulein, R., Guye, P., Rhomberg, T.A., Schmid, M.C., Schroder, G., Vergunst, A.C., Carena, I., and Dehio, C. (2005). A bipartite signal mediates the transfer of type IV secretion substrates of *Bartonella henselae* into human cells. P Natl Acad Sci USA *102*, 856-861.